AIMS Materials Science, 6(3): 406–440.
DOI: 10.3934/matersci.2019.3.406
Received: 11 March 2019
Accepted: 04 May 2019
Published: 21 May 2019

http://www.aimspress.com/journal/Materials

Review

Functional behavior of AlF_3 coatings for high-performance cathode materials for lithium-ion batteries

Christian M. Julien* and Alain Mauger

Sorbonne Université, Institut de Minéralogie, de Physique des Matériaux et de Cosmochimie (IMPMC), CNRS UMR 7590, 4 place Jussieu, 75005 Paris, France

*** Correspondence:** Email: christian.julien@upmc.fr.

Abstract: In response to the ever worsening of the environment by consumption of fossil fuels, energy storage systems like lithium-ion batteries that offer high energy efficiency have evoked a great interest as power sources from portable electronics to electric vehicles. However, the improvement of calendar and cycling life together with safety issues require sophisticated technology to prevent degradation mechanisms. The surface modification of the electrode materials is part of the solution. In this paper, the surface coverage of cathode materials by aluminum fluoride is reviewed. The effect of AlF_3 coating on electrochemical performance is examined at various deposit amounts with a comparison of the capacity retention and cycling stability of the different systems proposed in the literature.

Keywords: Li-ion batteries; cathode materials; aluminum fluoride coating; electrochemical performance

1. Introduction

The research on optimized electrode materials for Li-ion batteries aim at enhancing the energy density and the power density, improve the calendar and the cycling life, without compromising the safety of the cells [1]. In spite of these efforts, practical applications are still hindered by severe capacity fading during cycling and poor rate capability due partly to side reaction at the electrolyte–electrode interfaces (EEI). During long-term cycling, several unwanted degradation mechanisms occur (Figure 1a) such as oxidation of the electrolyte at high potentials, formation and growth of the solid electrolyte interphase (SEI), transition-metal dissolution, growth of a layer-to-spinel surface

layer, unreacted residual lithium ingredients on the particle surface (i.e., LiOH, Li_2CO_3, which are dominant with Ni-rich oxides), formation of corrosion pits and occurrence of inter-granular cracks inside primary particles and severe etching/corrosion by the acidic species in the electrolyte (HF attack) [2–8]. Note that the formation of HF originates from the reaction of the lithium salt $LiPF_6$ used in common electrolyte of Li-ion cells and trace amounts of water (or alcohols) described by [9]:

$$LiPF_6 + H_2O \rightarrow LiF + POF_3 + 2HF \quad (1)$$

The existence of water, even in very small concentration, generates HF and causes breakdown of the electrolyte. If decomposition of the electrode material occurs by HF attack, byproducts are inevitably gathered. During extensive cycling, the HF attack on $LiCoO_2$ electrode, for instance, can generate byproducts from Co on the surface of active particles. Then, these byproducts having Co–F bonding can be detected by spectroscopy assuming the relations [10]:

$$LiCoO_2 + 2HF \rightarrow CoO + LiF + H_2O \quad (2)$$

$$CoO + 2HF \rightarrow CoF_2 + H_2O \quad (3)$$

These byproducts would adhere at the surface of the separator and enhance the internal resistance of the Li//$LiCoO_2$ cell.

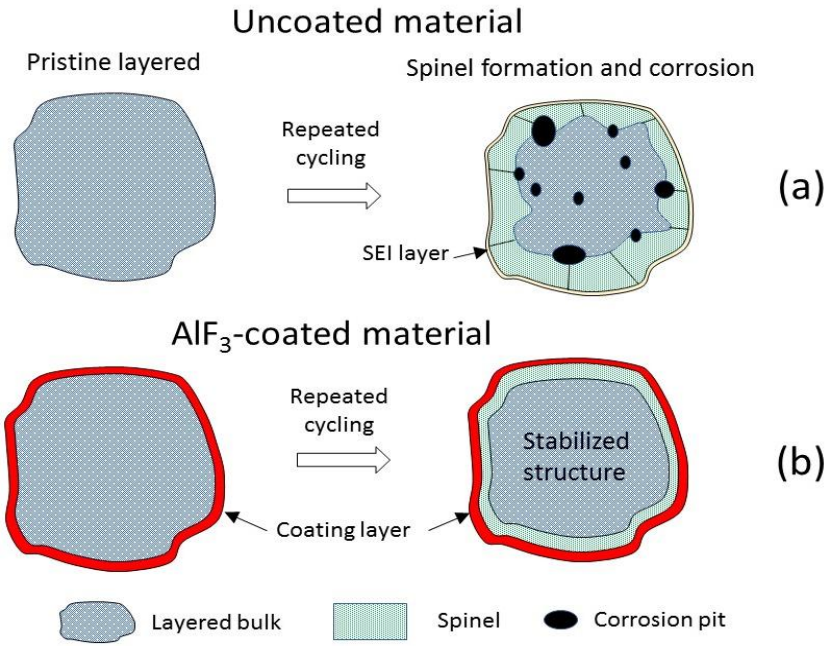

Figure 1. Scheme of transformation of active particle of Li-rich layered oxide upon repeated cycling. Reproduced with permission from [8]. Copyright 2014, American Chemical Society.

Several strategies have been directed to ameliorate the cycling performance of cathodes. Four representative tactics are currently used: (i) surface coating/modification [11,12], partial substitution of cations [13], partial substitution of oxygen anion [14] and utilization of electrolyte additives [15]. Moreover, some works have successfully associated doping and coating to enhance the electrode performance [16,17]. In most cases, surface engineering was realized by the deposition of a thin

protective layer that covers uniformly the active particles (Figure 1b). Optimizing the surface region of a layered oxide is of prime importance because the outer area of a particle experiences the Li-ion path for insertion/deinsertion reaction. Hashem et al. [18] demonstrated that one function of coating is the crystallization of the thin disordered layer on the surface of $LiNi_{1/3}Co_{1/3}Mn_{1/3}O_2$, which improves the electrochemical properties. Other functions of the coating layer can be described considering two mechanisms: (i) the coat acts as a barrier to the electrolyte infiltration effect that reduced the electrolyte-electrode reactions and (ii) the coating works as an HF scavenger. Numerous oxide materials used as protective coatings have proved to maintain the stability of the electrode–electrolyte interface in Li-ion batteries [11,12].

Electrode materials have been successfully coated with metal fluorides, i.e., LaF_3, MgF_2, ZrF_4, CaF_2, SrF_2, YF_3, AlF_3 [19–28], and metal oxyfluorides, i.e., ZrO_xF_y, BiOF and YOF [29–31]. Generally, fluoride coatings demonstrate higher stability than most metal-oxide coats and potent erosion resistance against the HF in the electrolyte. Lee and Park [22] showed that a MgF_2 coating layer deposited by co-precipitation technique onto $LiCoO_2$ thin-film electrode reduces the dissolution of Co and the surface damage during cycling at 45 ℃. The 1 wt% MgF_2 coating of $LiCoO_2$ by chemical deposition improves the electrochemical performance with was optimized of MgF_2 but fails to increase significantly the thermal stability [32]. The crystalline 2 mol% SrF_2 coating on $LiMn_{1/3}Ni_{1/3}Co_{1/3}O_2$ (NMC333) powders suppresses the increase of the charge-transfer resistance during cycling over the voltage window 2.5–4.6 V vs. Li^+/Li [26]. Coating NMC333 with LiF eliminates the increase in the charge transfer resistance that occurs for long cycling and during storage in the charged state [33]. Coating $LiCoO_2$ particles with ZrO_xF_y by a chemical deposition method leads to similar results, in which case the ZrO_xF_y deposit was obtained via adding NH_4F in Zr^{4+} aqueous solution with a controlled Zr:F ratio of 1:4 [29].

Note, however, that the beneficial effect of the layer coating is strongly dependent on the nature and morphology of the coating material. As the MF_3 fluorides are more stable than most of the other compounds under the corrosion of HF, the main effect of the coating with fluorides is an improvement of the electrochemical performance owing to the decrease of the dissolution of the active electrode material and protection against HF attack. Indeed, LaF_3 coating has significantly improved both the rate capability and the cycling performance of $LiCoO_2$ [19] and $LiMn_2O_4$ [34] as well. Another good reason to use AlF_3 as a buffer layer is its excellent protection for the aluminum collector from corrosion by the conventional electrolyte including $LiPF_6$ as the lithium salt. Moreover, Al is a light and cheap element. These features explain the superiority of AlF_3 and its success over the other metal fluorides as a protective coat of the electrode materials.

Metal fluorides can be used in lithium batteries in many ways. On a historical point of view, they have first been studied already in the 1960s for application as electrodes in primary lithium batteries, because they act as conversion materials, forming lithium fluoride during discharge, leading to large capacities and energy densities reported in different reviews [35,36]. However, the huge change of volume associated to the conversion reaction and the fact that the reaction is only partially reversible prevent their practical use as electrodes for secondary (i.e., rechargeable) batteries. Some recent progress has been made by mixing nanoparticles of metal fluorides such as BiF_3, FeF_2, FeF_3 [37,38] and AlF_3 [39] with carbon to buffer the product of the reaction. However, LiF is a product of the conversion reaction, which is one of the most insulating material on earth, which results in large overpotentials and high resistance, so that the electrode works only at very low C-rates, i.e., at very small currents. For example, the AlF_3–carbon composite only works at 0.1C, and

still only 4% of the initial capacity is maintained after 10 cycles [39], precluding the practical use of this material as an electrode in the rechargeable lithium-batteries considered here. In practice AlF_3 is suitable only for electrode protection because it is rather inert and the Al^{3+}-ion cannot be reduced or oxidized in battery conditions [11].

Hereunder, we review the different effects of AlF_3 coating, namely (1) electrode protection agent, (2) safety protection medium, (3) Al corrosion inhibitor, and (4) HF scavenger, and the resulting improvement of the electrochemical performance depending on the cathode material. After a brief description of the AlF_3 phase including synthesis methods and transport properties, we consider the different AlF_3-coated materials used in Li-ion batteries.

2. Aluminum fluoride coating material

2.1. Structural properties of AlF_3

Aluminum fluoride possesses five known varieties, i.e., α-, β-, η-, κ-, τ-AlF_3 [40], out of which α-AlF_3 is the most thermodynamically stable phase (perovskite-like form). It crystallizes with a rhombohedral structure (space group R-3*c*) and is thermodynamically stable at room temperature. The lattice has two equivalent stable interstitial sites per primitive cell, which can be occupied by lithium ions; they are located at the center of each distorted cube of α-AlF_3 at (¼,¼,¼) and (¾,¾,¾) coordinates. The β-AlF_3 metastable phase crystallizes with an orthorhombic structure (*Cmcm* space group). α-AlF_3 is a dielectric compound with a low refractive index, wide bandgap ~10.8 eV and strong Lewis acidity [41]. Due to its interesting optical, electrical and magnetic properties, a metal fluoride such as AlF_3 is an interesting compound for a wide variety of applications including optical designs, ionic conductors, protective coatings for electrodes in Li-ion batteries, heterogeneous catalyst and ferroelectric components [42–44]. With a low Gibbs free energy of formation, the advantage of AlF_3 against the amphoteric Al_2O_3 coating has been demonstrated from the exposure to trace of HF [45]. Therefore, a non-negligible advantage is that the AlF_3 coating layer appears to be a good Li^+-ion conductor after lithiation. Interestingly, $LiPF_6$ is the lithium salt actually used in the commercial Li-ion batteries. $LiPF_6$ is chosen not only because the very good ionic conductivity, but also due to its ability to form an AlF_3 layer protecting the aluminum current collector against electrolyte corrosion. The efficient effect of passivation of the current collector surface by AlF_3 coat is known since a long time [46,47].

The corrosion of Al current collector (CC) foil has been recently revisited by Ma et al. [48]. The natural Al_2O_3 passivation layer promotes the deprotonation of the cationic radical of ethylene carbonate (EC^+), which provokes the decomposition of PF_6^- anion and forms a proton-resistive AlF_3 layer on the Al surface. XPS measurements of the binding energy show that a CC foil anodized at 3.9 V for 20 h displays the conversion of the Al_2O_3 layer (75.6 eV) to stable AlF_3 passivation film (77.2 eV). Methyl difluoroacetate is used as fluorinated solvent that facilitates the formation of AlF_3 to passivate the surface of Al foil [49].

2.2. AlF_3 deposition methods

Various methods have been utilized to prepare AlF_3-coated lithiated materials: (a) chemical deposition or coprecipitation process [45], (b) atomic layer deposition [50–53], and (c) solid-state

reaction [54]. The most popular technique used for AlF_3-coating is the chemical precipitation route. In this process, aluminum nitrate dehydrate, $Al(NO_3)_3$ and ammonium fluoride, NH_4F, are separately dissolved in distilled water as precursor solutions. The pristine powders are immersed in $Al(NO_3)_3$ dilute solution, whose pH is adjusted at value of 7.0 by adding ammonia solution, heated to 50 ℃ and stirred vigorously. NH_4F dilute solution is then added into the solution drop by drop. The molar ratio of Al to F is controlled to be 1:3, and the various amounts of AlF_3 are 2–15 wt% for coated Li-rich layered oxides. The mixed solution containing the cathode powders is stirred at 80 ℃ for 5 h to ensure the slow evaporation of solvent, and then dried at 60 ℃ in a vacuum oven. The final coated powders are obtained by heat treatment at 400 ℃ under flow of argon (or nitrogen) for 4 h to prevent the formation of Al_2O_3 and secure the formation of AlF_3-coated Li-rich oxide. The overall reaction for the AlF_3 deposit can be expressed by:

$$Al(NO_3)_3 + NH_4F \rightarrow AlF_3 + NH_4NO_3, \quad (4)$$

which occurs in the solution reaction at room temperature, and the departure of NH_4NO_3 during the heat treatment in nitrogen atmosphere at 400 ℃:

$$NH_4NO_3 \rightarrow NO_2 + NH_3 + H_2O. \quad (5)$$

In the atomic layer deposition (ALD) process, trimethylaluminum (TMA) and anhydrous hydrogen fluoride are developed for the deposition of AlF_3 at substrate temperatures between 100 and 200 ℃. Gaseous HF source (pressure of 10 kPa at room temperature) is HF-pyridine, which enables the safe handling of anhydrous HF [50]. A typical deposit process is designed by 1 s dose of TMA injection, 30 s of N_2 purge, 1 s dose of TMA injection and 30 s of N_2 purge that produces a linear growth of AlF_3 with a mass gain of ~30 ng cm^{-2} per cycle. Jackson optimized the ALD AlF_3 coating onto $LiNi_{0.5}Mn_{0.3}Co_{0.2}O_2$ cathode powders using a $Al(CH_3)_3/TaF_5$ precursor combination that obviates the utilization of highly toxic HF(*g*) [54]. The freestanding $LiCOO_2$/multiwall carbon nanotube (LCO-MWCNT) electrodes were coated with 2 ALD cycles of AlF_3 conducted at 150 ℃ [55]. TMA and HF derived from HF–pyridine solution were used as precursors in the ALD process according the reactions [51]:

$$AlF_3\text{-}HF + Al(CH_3)_3 \rightarrow AlF_3\text{-}AlF(CH_3)_2 + CH_4, \quad (6)$$

$$AlF(CH_3)_2 + HF \rightarrow AlF_3\text{-}HF + CH_4, \quad (7)$$

showing that $AlF(CH_3)_2$ fluorinated by the HF exposure is the key intermediate reaction to produce AlF_3 growth. The AlF_3 coating realized by solid-state reaction consists in the sintering at 970 ℃ for 15 h of the mixture of AlF_3 powder (particle size ~400 nm) with the precursor of the electrochemically active material and Li_2CO_3 (5 wt% excess) [54]. AlF_3- and LaF_3-coating $LiCoO_2$ electrodes were also prepared by spin-coating method and thermally treated at 400 ℃ for 30 min [56].

2.3. Transport in AlF_3 coating

Lithium transport through surface coatings has been theoretically examined by several groups using first-principles calculations based on density functional theory [57–59]. A host supercell containing diluted concentration of Li atoms was considered for amorphous AlF_3 (a-AlF_3) with N_{Li}/N_{host} ratio of 100:80,000 [57]. The self-diffusion coefficient (D_s) vs. temperature was represented by an Arrhenius law:

$$D_s = D_0 \exp[-E_{eff}/k_B T], \quad (8)$$

where D_0 is the diffusion prefactor and E_{eff} the effective activation barrier, with the fitting parameters $D_0 = 7.7 \times 10^{-9}$ m^2 s^{-1} and $E_{eff} = 0.65$ eV for a-AlF_3 coating (Figure 2). Xu et al. [59] studied the diffusivity of interstitial lithium in crystalline α-AlF_3 and amorphous a-AlF_3. For an electronically insulating conformal coating, the transport of Li^+ ions, which are the unique mobile charge species, is driven by an electric field. To balance the positive charge of Li^+, there is a compensating negative charge in the coating, which is assumed to be immobile. This model referred to as "electrolyte model" [59] has been shown to be consistent with experimental works [60–62]. Li ions can diffuse by hopping from one interstitial site surrounded immediately by 8 oxygens to nearest site at a distance of 3.59 Å throughout a saddle point and must cross a barrier height $E_m = 0.929$ eV in the process. Predicted transport properties for crystalline and amorphous AlF_3 coatings are summarized in Table 1 [59], which illustrates that the lithiated AlF_3 contains Li–Al–F bonds and acts as a stable lithium conducting solid electrolyte. A mechanism has been proposed for the accommodation of the Al-F coating at the electrode interface [63]. As a consequence of the small charge transfer resistance, the Al-F coating layer facilitates the Li^+ insertion/extraction at the interface. After heat treatment, the coating film is formed with an inner amorphous Li-Al-F layer such as $LiAlF_4$, which has been reported as a good lithium fast-ion conductor with a conductivity of 1×10^{-4} S m^{-1} at 25 °C [63]. The $LiAlF_4$ structure is constituted by a network of corner sharing AlF_6 octahedra and Li ions are primarily associated with non-bridging fluorine atoms [64,65]. Among the thermodynamically possible reactions, AlF_3 converts to the high intrinsic Li-ion conducting Li_3AlF_6 according to:

$$AlF_3 + 1.5Li \rightarrow 0.5Li_3AlF_6 + 0.5Al, \quad (9)$$

at potential $E = 1.28$ V Li^+/Li [66]. Li_3AlF_6 is a stoichiometric ternary mixture of LiF and AlF_3 exhibiting a high ionic conductivity of 10^{-6} S cm^{-1} [67]. Therefore, the morphology and microstructure of the final phase of AlF_3 are affected by the deposition methods. As an amorphous-like phase is requested for preventing low migration barrier values, using a moderate post heat-treatment of the AlF_3 deposit, the co-precipitation synthesis is the best method that generates a non-crystallized material. Similar precautions are currently taken into account for coating made by ALD technique, for which a low substrate temperature is maintained below 200 °C. The amorphous state of AlF_3 coating has been evidenced by several authors using HRTEM measurements (see Ref. [8] for example).

Table 1. Predicted transport properties for crystalline (α-AlF_3) and amorphous (a-AlF_3) coatings. Reproduced with permission from [57]. Copyright 2013, American Chemical Society.

Material	Diffusivity (cm^2 s^{-1})	Migration barrier (eV)	Conductivity at 25 °C (S cm^{-1})
α-AlF_3	6.2×10^{-18}	0.929	5.9×10^{-11}
a-AlF_3	9.3×10^{-16}	0.65	8.8×10^{-9}

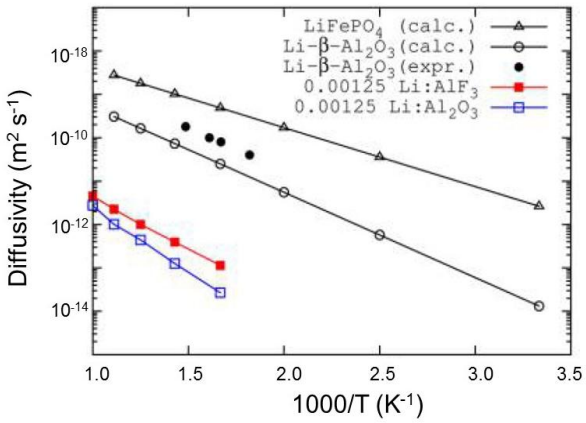

Figure 2. Calculated Li^+ ion self-diffusivity in a-Al_2O_3, a-AlF_3, and Li-β-alumina. A host supercell containing diluted concentration of Li atoms was considered for amorphous layers with N_{Li}/N_{host} ratio of 100:80,000 atoms. Reproduced with permission from [57]. Copyright 2013, American Chemical Society.

2.4. Relative energies in Li-ion battery

Figure 3 is a schematic representation of the relative energies in a Li battery. The equilibrium working voltage V^0 is given by the difference in chemical potential between anode (μ_A) and cathode (μ_C) for a given redox couple, i.e., 3.6 V vs. Li^+/Li for the $Ni^{2+/3+}$ couple in the $LiNi_{1/3}Mn_{1/3}Co_{1/3}O_2$ host [1]. The electrochemical stability of a Li battery is determined by the electrochemical stability window (ESW) of the electrolyte or bandgap energy E_g:

$$E_g = E_{HOMO} - E_{LUMO}, \tag{10}$$

where E_{HOMO} and E_{LUMO} are the energy of the highest occupied molecular orbital (HOMO) and the lowest unoccupied molecular orbital (HOMO), respectively. The condition for stability is given by:

$$E_g > (1/nF)\,(\mu_A - \mu_C), \tag{11}$$

where n is the number of electrons involved and F is the Faraday constant. Since μ_A of the lithium anode lies above the LUMO, the electrolyte is reduced to form a passivating SEI film that allows the diffusion of Li ions through the layer under a uniform electric field and prevents the decomposition of the electrolyte. On the cathode side, μ_C acts as a redox couple for the active transition-metal cation containing localized *d*-electrons in the *d*-manifold, e.g., $Ni^{2+/4+}$ in the NMC host material. During the charge/discharge process, the Fermi level E_{FC} is moved from one formal electronic state to another upon oxidation/reduction of the host. However, for the positive electrode in the charged state (E > 4.5 V), E_{FC} approaches the bottom of the $Co^{3+/4+}$ redox couple (μ_{Cc} potential), which interferes with the top of the anion *p* band (O^{2-}: $2p^6$) of the host and destabilizes the host by release of oxygen [68]. At this point, the cell voltage is also limited by the ESW of the electrolyte and a situation becomes similar to the anode side: μ_{Cc} lies below the HOMO level (located at 4.3 eV below $\mu_{A(Li)}$) implying decomposition of the electrolyte unless a passivating SEI film blocks the reaction [69]. A thin insulating layer applied on the surface of the cathode acting as buffer isolates the host from the electrolyte. As shown in Figure 3, the AlF_3 coating possessing a bandgap of

10.8 eV has an E_{HOMO} energy level much lower than that of the electrolyte, even in the upper state of charge (SOC) of the cathode. Note that cyclic voltammetry shows the ESW of $LiAlF_4$ is 2.75–4.5 V vs. Li^+/Li. However, the presence of such a film causes an increase in the internal resistance of the cell and consumes a portion of the lithium amount of the cathode [70].

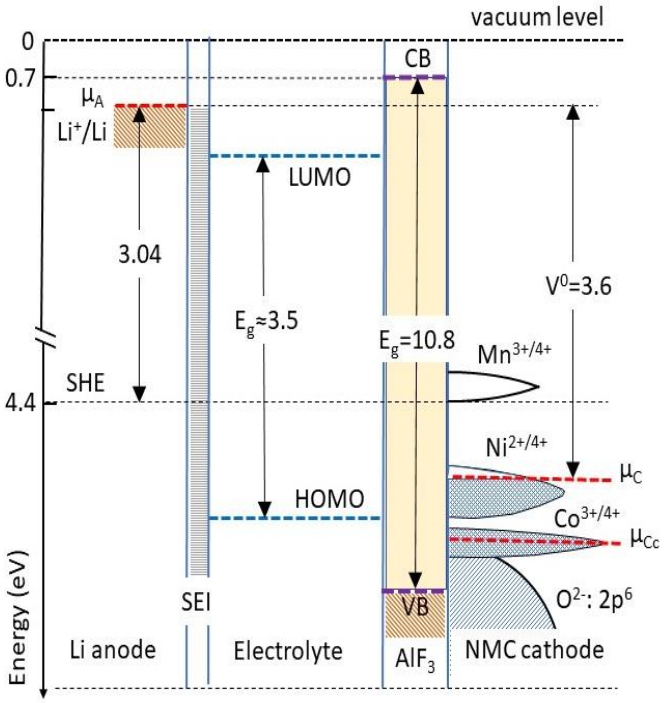

Figure 3. Scheme of the relative energies in a Li//NMC rechargeable battery showing the electrolyte window, E_g, and the HOMO and LUMO levels of the AlF_3 coating on the NMC cathode surface.

3. AlF_3-coated materials for Li-ion batteries

AlF_3 coating was used to enhance the performance of various cathode materials for Li-ion batteries including layered structures such as $LiCoO_2$ (LCO) [28,53,71–73], $LiNi_{1-y}Mn_yO_2$ (NMO) [74,75], $LiNi_xMn_yCo_zO_2$ (NMC) [76–86], Li-rich NMC (LNMC) [54,66,75,87–99], $LiNi_{1-x-y}Co_xAl_yO_2$ (NCA) [100–104], spinel structures such as $LiMn_2O_4$ (LMO) [105–110], $LiNi_{0.5}Mn_{1.5}O_4$ (LNM) [111–113], olivine structures $LiFePO_4$ (LFP) [114–116] and $LiCoPO_4$ (LCP) [117]. AlF_3 coating has been also experimented on anode materials such as graphite and $Li_4Ti_5O_{12}$, in which case the deposit suppresses the gas generation [118–121].

3.1. AlF_3-coated LCO

LCO cathodes show significant degradation of electrochemical behaviors above 4.5 V. At such high voltage, AlF_3 coating is a solution, while Al_2O_3 is not, because of the partial conversion of the layer to metal fluoride by HF attack producing H_2O [122]. The beneficial effect of the surface modification of LCO particles by AlF_3 coating was first reported by evaluating laminated-type full

Li-ion cells [123]. While the capacity of the uncoated LCO/C cell vanished rapidly after 500 cycles, the AlF_3-coated LCO cell showed excellent capacity retention of 91% at 1C rate in the range 3.0–4.5 V. Following this report, early analyses of AlF_3 coating on $LiCoO_2$ cathode particles was reported in Refs. [28,71]. The 0.5 mol% AlF_3 deposit shows a thin layer (5–10 nm thick) on the surface of $LiCoO_2$, which becomes thicker around 20–30 nm when the coating amount is 1 mol% [28]. This small deposit amount is sufficient to realize good performance with capacity retention of 97.7% after 50 charge–discharge cycles and capability of 93.1% at 5C rate. An LCO electrode coated with 2 mol% AlF_3 was able to deliver 208 mAh g^{-1} at 4.54 V upper cutoff voltage. The amount of Co dissolution of this electrode charged at 4.5 V as a function of the storage time in electrolyte at elevated temperature of 55 ℃ was compared with that of pristine material. Results show a concentration of 47 ppm for pristine LCO stored for 6 weeks, against only 19 ppm for the coated electrode [72]. DSC measurements of $LiCoO_2$ electrodes charged at 4.4 V and uniformly encapsulate by a 10–15 nm thick AlF_3 layer show that the exothermic peak associated with the thermal decomposition is at 273.5 ℃ and the reaction enthalpy is 392 J g^{-1}, against 208.5 ℃ and 544 J g^{-1}, respectively, for the bare materials [73]. This result demonstrates that the AlF_3 layer improves the thermal stability. This AlF_3-coated electrode allows a charge regime at high voltage of 4.6 V vs. Li^+/Li delivering a specific capacity of 160 mAh g^{-1}. Recently, Zhou et al. [53] fabricated freestanding $LiCoO_2$/multiwall carbon nanotube nanocellulose fibril (LCO-MWCNT-NCF) composite electrodes coated with AlF_3 layer. The AlF_3 deposit was realized with 2 ALD cycles, leading to a high specific capacity of 216 mAh g^{-1} at 4.7 V for LCO-MWCNT-NCF electrodes. In contrast, when coated with 2 ALD cycles of Al_2O_3, LCO-MWCNT-NCF electrodes cannot be cycled above 4.5 V due to the higher LUMO energy level.

3.2. AlF_3-coated NMO

The single-phase $LiNi_{1-x}Mn_xO_2$ (NMO) exhibits a specific capacity of 150 mAh g^{-1} with the formal charges of Ni and Mn of 2+ and 4+, respectively, only the $Ni^{2+/4+}$ redox couple being available. However, the electrochemically inactive Mn^{4+} provides significant structural stability [124]. $LiNi_{0.5}Mn_{0.5}O_2$ cathode materials prepared by quenching treatment and coated with AlF_3 by conventional coprecipitation method show initial discharge capacity of 175 mAh g^{-1}, decreasing to 153 mAh g^{-1} after 50 cycles at 0.1C rate (28 mA g^{-1}). At high current density of 5C rate (1.4 A g^{-1}), this coated electrode delivered 120 mAh g^{-1} at in the voltage range 2.5–4.5 V [125]. Time-of-flight secondary ion mass spectroscopy was used to investigate the effect of a ~10 nm AlF_3 deposit on $LiNi_{0.5}Mn_{0.5}O_2$ electrode [74]. The insulating LiF outer layer originating from the $LiPF_6$ decomposition was suppressed by the AlF_3 coating with the benefit of the reduction in the charge transfer resistance. Figure 4 shows the electrochemical features of pristine and AlF_3-coated $Li[Ni_{0.5}Mn_{0.5}]O_2$. The surface modification using 2 wt% AlF_3 of layered oxide improved significantly the cycling stability of the electrode [75], which retained a specific capacity of 175 mAh g^{-1} after 50 cycles at C/2 rate in the voltage range 2.0–4.4 V (Figure 4a). This corresponds to a capacity retention of 93% with an excellent coulombic efficiency of 99.5% much higher than that of the pristine material (Figure 4b).

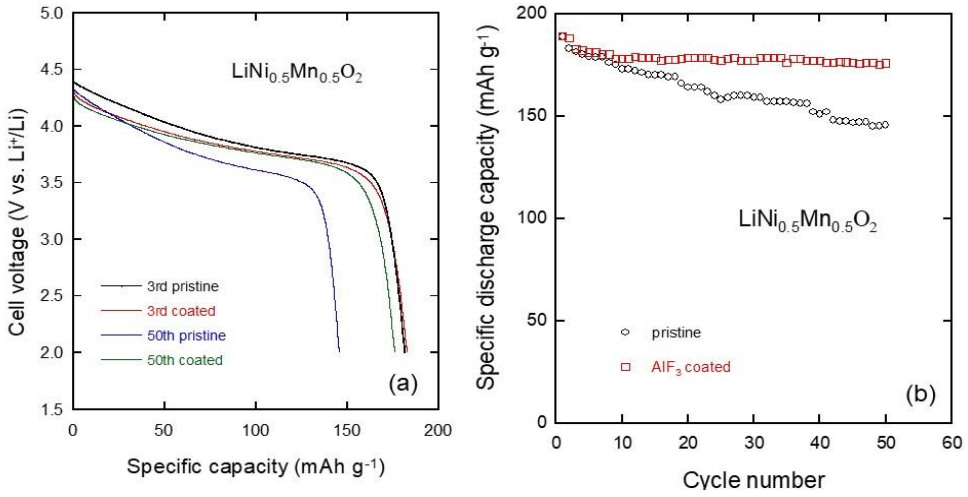

Figure 4. Electrochemical performance of pristine and AlF_3-coated $LiNi_{0.5}Mn_{0.5}O_2$ (a) discharge profiles carried out at C/2 rate and (b) cycleability. Reproduced with permission from [75]. Copyright 2019, Elsevier.

3.3. AlF_3-coated NMC

Cathodes based on $Li[Ni_xMn_yCo_z]O_2$ (NMC) compounds with $x + y + z = 1$ are actively studied as the new generation of stable high-specific-energy cathode materials for Li-ion batteries [126]. In an early work, Woo et al. [76] investigated the electrochemical performance of the AlF_3-coating of Ni-rich $LiNi_{0.8}Co_{0.1}Mn_{0.1}O_2$ (NMC811) cathode materials and examined the stabilized electrolyte/electrode interface. A 10-nm thick coating on NMC333 powders was obtained using 0.25 mol% of AlF_3 in the sol-gel solution [77,78]. Regardless the cycle life of AlF_3-coated $LiNi_{1/3}Co_{1/3}Mn_{1/3}O_2$ electrodes, Sun et al. [77] determined that the charge transfer resistance (R_{ct}) was stable under the high voltage cutoff of 4.6 V. The surface of the layered $LiNi_{1/3}Co_{1/3}Mn_{1/3}O_2$ cathode materials was modified by covering the particles with a 10 nm thick AlF_3 layer deposited by the conventional coprecipitation technique. Electrochemical tests showed an improvement of the performance at high cutoff voltage of 4.5 V, with a capacity retention of 81% after 800 cycles and a decrease of the area specific impedance even at the discharge rate of 10C [79]. About 3 nm thick uniform AlF_3 coating (1.5 wt%) on the surface of $LiNi_{1/3}Co_{1/3}\ Mn_{1/3}O_2$ limited the capacity fading at 3% when cycled 80 times in the voltage range 2.8–4.3 V at 2C rate [80], which is better than the 93.5% capacity retention obtained at 1C at 60 °C after 50 cycles for the LiF-modified $LiNi_{1/3}Co_{1/3}\ Mn_{1/3}O_2$ electrode [81]. AlF_3-coated $LiNi_{0.45}Mn_{0.45}Co_{0.10}O_2$ as cathode material [82] delivered an almost stable specific capacity of ~145 mAh g^{-1} when discharge at the rate of 0.1C (20 mA g^{-1}) in the voltage range 2.5–4.5 V. The thermal behavior of AlF_3-coated $Li_xNi_{1/3}Co_{1/3}Mn_{1/3}O_2$ was studied in the charged state, i.e., in the delithiated Li concentration $x = 0.35$. TGA and high-temperature XRD data showed that the phase transition from rhombohedral $Li_{0.35}MO_2$ to spinel $Li_{0.7}M_2O_{1.933}$ structure appearing at 450 °C is induced by a slight amount (~0.07 mol) of released oxygen. The decrease of oxygen loss (~0.04 mol) was detected for the AlF_3-coated $Li_{0.35}Ni_{1/3}Co_{1/3}Mn_{1/3}O_2$ electrode, which retards the formation of the spinel phase. It was concluded that the AlF_3 coating layer played two roles at the particle surface: (i) a protection against oxygen loss and (ii) a sacrificing for the formation of Li-Al-O and Li-Al-F complexes [83]. Using dual

deposition process of metal fluorides, the co-effect of 1 wt% AlF_3 and 1 wt% MgF_2 coated layers on the electrochemical properties of NMC333 was studied under high voltage in the range 2.8–4.7 V. In that case, the coated electrode delivered an initial capacity of 207 mAh g^{-1} at C/5 discharge rate [127]. Commercial $LiNi_{0.5}Mn_{0.3}Co_{0.2}O_2$ powders (NMC 532, from ECOPRO Co., Korea) were coated with either AlF_3 or $LiLaPO_4$ to fabricate a blended cathode [84]. The synthesis was realized with 0.25 wt% AlF_3 of the NMC532 powder in the solution, which increases the thermal stability of the electrode charged at 4.6 V. Owing to the coating, the exothermic DSC peak shifts from 230 to ~280 ℃ and the heat generation decreases from 186 to 100 J g^{-1} compared to uncoated particles. Spherical NMC532 particles were coated with different AlF_3 concentrations in the molar ratio range 0.25–2.0 [85]. A combination of XRD data, galvanostatic charge/discharge tests and EIS measurements showed that 0.5 mol% AlF_3 coating is the best content providing a high specific capacity of ~160 mAh g^{-1} at 6C rate in the voltage range 2.8–4.5 V. Yang et al. [85] coated the surface of $LiNi_{0.5}Mn_{0.3}Co_{0.2}O_2$ (NMC532) by coprecipitation method, the amount of AlF_3 being set at molar ratios n_{AlF3}/n_{NMC532} in the range from 0.25 to 2%. It was demonstrated that oxygen vacancies favor the Li^+-ion transport and increase the capacity in forthcoming cycles. An important advantage of the AlF_3 coating layer is the termination of the increase of cell impedance upon charge–discharge process by preventing directly the SEI formation. The AlF_3-coated NMC532 operating at 4C over 2.8–4.5 V had capacity retention of 98% (initial specific capacity of mAh g^{-1}) after 100 cycles. Ni-rich $LiNi_{0.8}Mn_{0.1}Co_{0.1}O_2$ electrodes (NMC811) with AlF_3 interfacial layer deposited by ALD technique from $AlCl_3$ and TiF_4 precursors kept at 120–130 ℃ were investigated in the voltage range 2.75–4.5 V vs. Li^+/Li. The average specific capacity of AlF_3-coated NMC811 cathode was 184 mAh g^{-1} at 20 mA g^{-1} current density and 106 mAh g^{-1} at 200 mA g^{-1} [66].

3.4. AlF_3-coated Li-rich layered NMC cathodes

The lithium-rich $Li[Li_\delta Ni_x Mn_y Co_z]O_2$ (NMC) compounds with $\delta + x + y + z = 1$ layered oxides (LNMC) are inter-grown composite structures $xLi_2MnO_3 \bullet (1 - x)LiMO_2$ (M = Mn, Co, Ni), which have attracted a lot of interest as positive electrode (cathode) materials for Li-ion batteries because since the their high energy density of about 250 mAh g^{-1} in the voltage range 2.0–4.8 V vs. Li^+/Li [128]. Nowadays, they are considered as promising cathode element and used for powering electric vehicles (EVs). Surface analysis showed that surface-modified $Li[Li_{0.2}Ni_{0.17}Co_{0.07}Mn_{0.56}]O_2$ nanoparticles with 3 wt% of AlF_3 deposited by chemical process (2 nm thick) exhibits a largely suppression of the undesirable growth of SEI layer. This 3 wt% of AlF_3 coating enhanced the capacity retention to 83% and the cathode delivers a specific discharge capacity of 182 mAh g^{-1} after 50 cycles when charged to 4.8 V vs. Li^+/Li. In relation to the effect of the coating on the SEI formation, a detailed description of the complex surface chemistry of Li-rich layered cathodes can be seen in Ref. [86]. This decrease of impedance is responsible in turn for the improvement of the rate capability. For instance, the reversible capacity of the AlF_3-coated $Li(Li_{0.17}Ni_{0.25}Mn_{0.58})O_2$ at 5C rate was raised to 104 mAh g^{-1} after 200 cycles, much larger than before coating. Electrochemical tests exhibited improved rate capability and life cycle behavior at elevated temperature of 55 ℃ with the best results for 0.5 mol% of aluminum fluoride deposit. Furthermore, the thermal stability studied by DSC showed a shift of the exothermic peak from 247 to 308 ℃ with lower exothermic heat release [87]. Using a combination of scanning/transmission electron microscopy (SEM/TEM) and electron energy loss spectroscopy (EELS) characterizations, Sun et al. [45] evidenced that the

coating of $Li[Li_{0.19}Ni_{0.16}Co_{0.08}Mn_{0.57}]O_2$ cathode enhanced the overall electrochemical features in contrast with the typical shortcomings of Li-rich positive electrodes due to the Li chemical leaching effect of the AlF_3 deposit transforming the initial Li_2MnO_3 layer to a spinel phase. Optimized electrode with 2 wt% AlF_3 coating concentration delivered a specific capacity of about 206 mAh g^{-1} when cycled between 2.0 and 4.6 V at a current density of 0.5C rate (125 mA g^{-1}) over 100 cycles. From the thermal stability view point, the 2 wt% coating reduces the exothermic reaction with a generated heat of 274 J g^{-1} at 262.5 °C.

A core shell material $Li_{1.2}Mn_{0.54}Co_{0.13}Ni_{0.13}O_2@AlF_3/C$ (LMSAC) was synthesized by coating AlF_3 and carbon hybrid deposit via sol-gel process. The LMSAC cathode delivered the initial specific capacity of 230 mAh g^{-1} at 1C rate in the potential range of 2.0–4.8 V vs. Li^+/Li and exhibited a capacity retention of 96% after 50 cycles [88]. The AlF_3 surface-treated $Li_{1.1}(Ni_{0.15}Co_{0.1}Mn_{0.55})O_{1.95}$ layered oxide was cycled at 25 and 55 °C. At elevated temperature, a capacity gain of 10% was attributed to the improved thermodynamic activation [89]. Li-rich Mn-based cathode $Li[Li_{0.2}Fe_{0.1}Ni_{0.15}Mn_{0.55}]O_2$ particles doped with iron were artificially protected by 7% AlF_3 nano-coating obtained by coprecipitation method [90]. It was stated that the fluorine source, NH_4F, acts as a chelating agent that promotes a slow reaction with aluminum and more complete coating film. Upon 3-nm AlF_3 coating, great structural changes were observed by TEM and electron diffraction measurements. An integrated layered-spinel structure was formed. An excellent performance with a specific capacity of ~120 mAh g^{-1} was observed after 100 cycles at 20C rate. As AlF_3 coat appeared to be uniform and thin (compared with the 15-nm Al_2O_3 layer), this protecting deposit is preferred to Al_2O_3 for the electrochemical behaviors that can be triggered by tuning the amount of coating. Zheng et al. [8] demonstrated the efficiency of AlF_3 coating on Li-rich Mn-rich $Li_{1.2}Ni_{0.15}Co_{0.10}Mn_{0.55}O_2$ electrode cycled at C/3 rate in the voltage range 2.0–4.75 V vs. Li^+/Li upon cycle number. Quantitative analysis of the pre-peak of the O *K*-edge and the linear relation of L_3/L_2 EELS intensity with the Mn valence state at the particle surface and in the bulk showed the reduced formation of oxygen-deficient surfaces and the stabilization of the spinel-like phase (Figure 5).

$Li_{1.17}Ni_{0.25}Mn_{0.58}O_2$ with 5–7 nm thick AlF_3-coating provided a high specific capacity >250 mAh g^{-1} at 0.2C rate, maintained at 104 mAh g^{-1} when discharged high current density of 5C after 200 cycles. Such a material displayed improved coulombic efficiency from 76.4 to 89.5%. EIS analyses revealed that the AlF_3 layer induces a pre-activation of the Li-rich layered oxide with a maintenance of more active Li sites during the insertion/extraction reaction [91]. The effects of AlF_3 modifying cyclic performance of $Li_{1.24}Ni_{0.12}Co_{0.12}Mn_{0.56}O_2$ cathode materials (LNCM@AlF_3) were recently reported by Ding et al. [92]. A combined set of electrochemical tests showed that the best results are obtained with a proper coating of 2 mol% AlF_3 (~7 nm in thickness). This homogeneous layer favored the diffusion ability of Li^+ ions at the electrode/electrolyte interface and largely decreased R_{ct} from 350 Ω in pristine to 59 Ω in LNCM@2%AlF_3 electrode. LNCM@2%AlF_3 operating at 55 °C delivered a specific discharge capacity of 219 mAh g^{-1} at current density of 20 mA g^{-1} after 50 cycles. Kim et al. [63] reported the positive effect of a controlled AlF_3 coating on the Li-rich NMC electrode, namely $0.5Li_2MnO_3•0.5LiNi_{0.5}Mn_{0.3}Co_{0.2}O_2$ (or $Li_{1.2}Mn_{0.52}Ni_{0.2}Co_{0.08}O_2$). The authors attributed this improvement to the fact that the coating (nominal amount of AlF_3 about 0.25 mol% of the LNMC material) leads to a Li–Al–F interface that acts as a stable lithium conducting solid electrolyte. At discharge rate of 0.5C in a voltage range of 2.0–4.6 V vs. Li^+/Li, the Al-F coated electrode had an improved capacity retention (98% of the 216 mAh g^{-1} initial capacity) compared to the pristine one (93% of the 206 mAh g^{-1} initial capacity).

The surface modification of $Li[Li_{0.11}Ni_{0.33}Mn_{0.56}]O_2$ with various amounts of AlF_3 ($0 \leq AlF_3$ mol% ≤ 10) was realized by the precipitation routine setting the Al:F ratio to 1:3. After coating with 5% Al/F and heat treatment at 400 ℃, the particle had a core-shell structure: a disordered layer separated the crystalline LNMC bulk from the amorphous AlF_3 outer coating. The electrode with low coating content (~1 mol%) had a specific capacity of 215 mAh g^{-1} on charging to 4.6 V [93]. Wang et al. [94] claimed excellent electrochemical behaviors of the AlF_3-coated $Li_{1.2}Mn_{0.534}Ni_{0.133}Co_{0.133}O_2$ cathode that exhibited a discharge capacity of 222 mAh g^{-1} (capacity retention of 96.5%) after 50 cycles at 1C rate. Li et al. [95] prepared an AlF_3-coated $Li_{1.2}(Mn_{0.54}Ni_{0.16}Co_{0.08})O_2$ cathode materials via wet process. Optimized powders with 5–7-nm thick AlF_3 layer exhibited a capacity retention of 72.4% after 50 cycles at 1C rate. Amalraj et al. [86] considered the detailed chemistry of the coating/active material and the electrochemical performance of Li and Mn rich $xLi_2MnO_3 \bullet (1-x)LiMn_yNi_zCo_wO_2$ powders ($0.4 \leq x \leq 0.5$) with an emphasis on the effect of 2–3 wt% AlF_3 coating. TEM studies showed that the coating layer is formed of nano-crystals with tetragonal structure t-AlF_3 (*P*4*nmm* space group) regularly distributed. Additionally, amorphous clusters Al-containing species, like AlF_3, AlF_xO_y and Al[FOH] were detected by solid-state NMR measurements. Such AlF_3-coated material exhibited specific capacity of ~250 mAh g^{-1} at a C/5 rate, and high lithium storage capability at 60 ℃. Li- and Mn-rich layered oxide $Li_{1.4}Ni_{0.25}Co_{0.10}Mn_{0.65}O_2$ was coated with a small amount of AlF_3 (~11 vol%) by the conventional sol-gel route [96]. It was shown that during preparation the environmental Li excess caused the formation of Al_2O_3 and LiF that led the surface conversion from Li_2MnO_3 to self-generated $LiMn_2O_4$ spinel layer, which upgrades the electronic conductivity of particles.

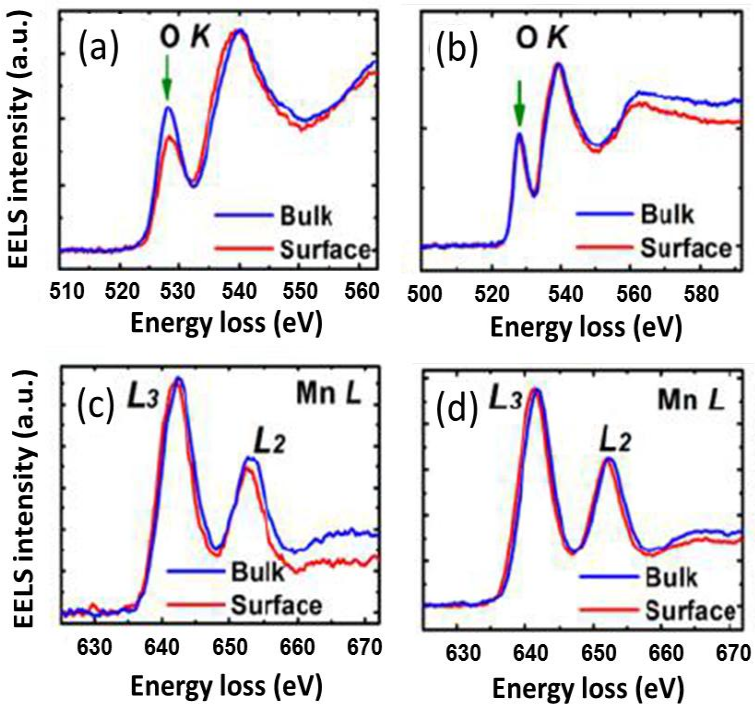

Figure 5. EELS experiments showing (a,b) the O *K* edge spectra, and (c,d) the Mn *L* edges spectra of the non-coated and AlF_3-coated $Li_{1.2}Ni_{0.15}Co_{0.10}Mn_{0.55}O_2$ particle boundary and the bulk of the particle, respectively. Reproduced with permission from [8]. Copyright 2014, American Chemical Society.

AlF_3 has been chosen as the inert coating material to protect the Li- and Mn-rich $xLi_2MnO_3•(1-x)LiMn_{0.5}Ni_{0.5}O_2$ particles with x = 0.3 ($Li_{1.134}Ni_{0.3}Mn_{0.566}O_2$) and x = 0.2 ($Li_{1.2}Ni_{0.2}Mn_{0.6}O_2$) [74]. Thickness of the amorphous AlF_3 coating layers (5 wt% of the Li-rich layered oxide) uniformly deposited by the conventional coprecipitation method is 5 nm for $Li_{1.2}Ni_{0.2}Mn_{0.6}O_2$ particles (200-nm size) against 2 nm for $Li_{1.134}Ni_{0.3}Mn_{0.566}O_2$ ones (Figure 6). Figure 7 presents the galvanostatic charge/discharge profiles carried out at *C*/10 rate (30 mA g^{-1}) in the potential range 4.5–2.0 V vs. Li^+/Li for (a) pristine and (b) AlF_3-coated $Li_{1.134}Ni_{0.3}Mn_{0.556}O_2$. The cell voltage vs. specific capacity of Li-rich layered oxides have been analyzed in prior works (see for instance Ref. [128]). The first discharge process occurs as activation of the rhombohedral $LiMn_{0.5}Ni_{0.5}O_2$ (*R*-3*m*) and monoclinic Li_2MnO_3 (*C*/2*m*) phases by several steps: (i) the delithiation of the *R*-3*m* phase with a voltage slope corresponding to the oxidation of Mn^{3+} and Ni^{2+} cations; (ii) activation of the *C*/2*m* phase at ca. 4.5 V associated with the oxygen loss; (iii) structural reorganization due to Li^+ ions removal evolving O_2. Following the first charge at ca. 5 V, the new active material contains presumably lithiated MnO_2 and $LiMn_{0.5}Ni_{0.5}O_2$ phase that provides a specific capacity of 230 mAh g^{-1} decreasing down 200 mAh g^{-1} after 55 cycles. The voltage fade issue was analyzed in terms of differential (or incremental) capacity as shown in Figure 8, which compares the $-dQ/dV$ vs. cell voltage plots of the 2nd and 50th cycle for bare and AlF_3-coated $Li_{1.2}Ni_{0.2}Mn_{0.6}O_2$. These graphs display a shift down to ~3.67 V after 50 cycles for the bare material, while stable voltage is shown for the coated electrode. All these results indicate that a 5-nm thick coating is enough to protect the electrode particle against the attack of the electrolyte.

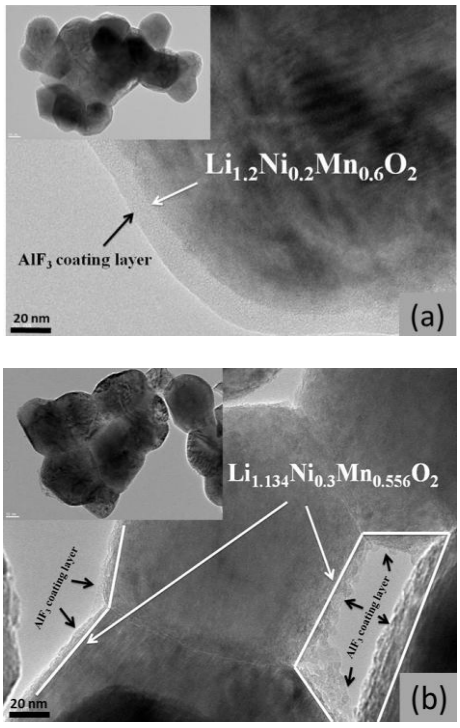

Figure 6. TEM images of $Li[Ni_xLi_{1/3-2x/3}Mn_{2/3-x/3}]O_2$ ($0 \le x \le 0.5$) powders. (a) AlF_3-coated $Li_{1.2}Ni_{0.2}Mn_{0.6}O_2$ and (b) AlF_3-coated $Li_{1.134}Ni_{0.3}Mn_{0.556}O_2$. Reproduced with permission from [75]. Copyright 2019, Elsevier.

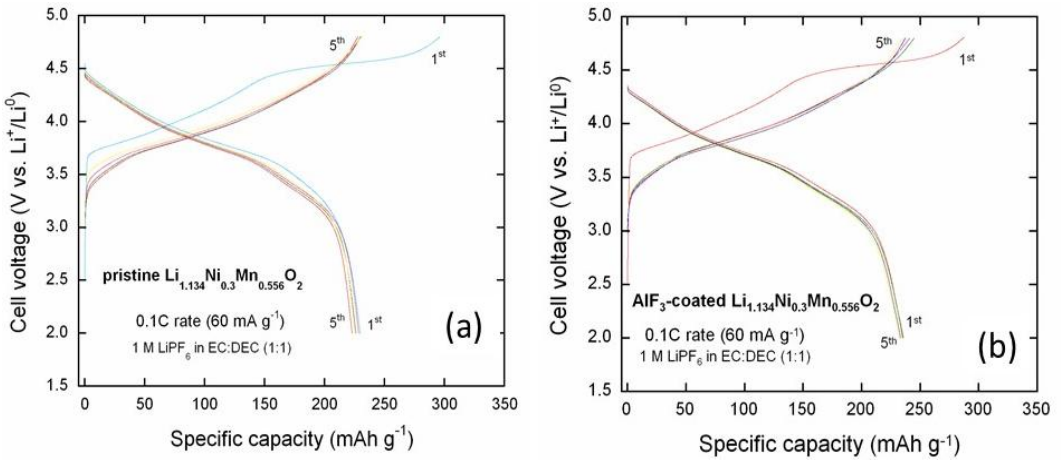

Figure 7. Galvanostatic charge/discharge profiles carried out at *C*/10 rate (30 mA g^{-1}) in the potential range 4.5–2.0 V vs. Li^+/Li for (a) pristine and (b) AlF_3-coated $Li_{1.134}Ni_{0.3}Mn_{0.556}O_2$. Reproduced with permission from [75]. Copyright 2019, Elsevier.

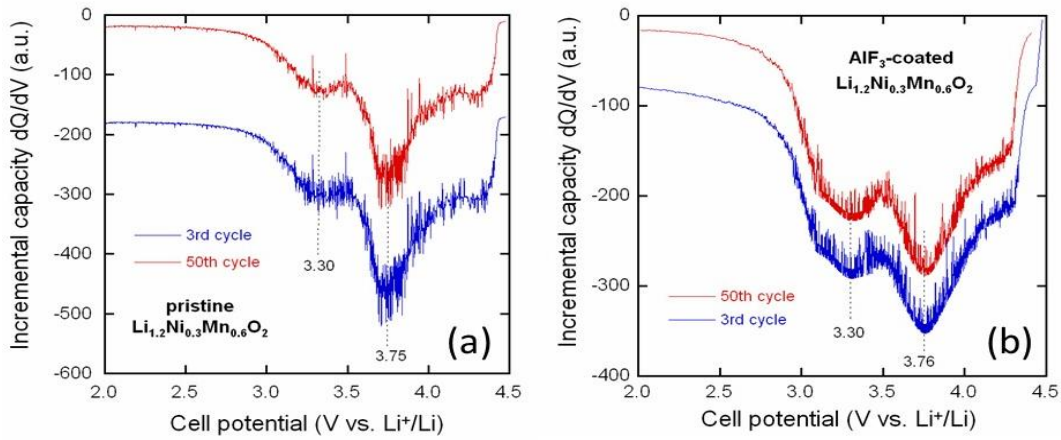

Figure 8. Differential capacity (−d*Q*/d*V*) plots of 2nd and 50th cycle for (a) pristine and (b) AlF_3-coated $Li_{1.2}Ni_{0.2}Mn_{0.6}O_2$. Reproduced with permission from [75]. Copyright 2019, Elsevier.

Zheng et al. [8] have investigated in more details the functional mechanism of the Li-rich and Mn-rich cathode materials, by a comparison between $Li_{1.2}Ni_{0.15}Co_{0.10}Mn_{0.55}O_2$ uncoated and coated with a 10 nm-thick AlF_3 layer. First, the AlF_3-coated material exhibited significantly reduced capacity decay above 3.5 V, like in Figure 9, indicating a reduction of layered to spinel-like phase transformation. Second, the AlF_3-coated material showed only 10.1% (0.40 V, inset of Figure 9) decrease in average discharge voltage after 100 cycles, which is smaller than the 12.3% (0.47 V) observed for uncoated material. This result, in agreement with other data [74,75], indicates that AlF_3 coating not only alleviates the undesirable phase transformation but also maintains the structural stability of the transformed spinel-like phase. The structural evolution of the coated and uncoated samples was investigated by S/TEM and EELS characterization in [8] after 100 cycles. The results are the following. In contrast with that of the uncoated sample, there is no serious corrosion observed for the AlF_3-coated material so that the cycling does not destroy the coat. There is no thick SEI layer

on the coated sample, the inert AlF_3 coat prevents direct contact between the electrode material and the electrolyte, which thus largely suppresses the side reactions between them observed in the uncoated sample. This result also proves that in spite of the oxygen extraction during activation of the Li_2MnO_3 component, the coating layer functions as a buffer layer to reduce the reactivity of evolved oxygen species and thus decrease the oxidation of electrolyte. Less oxidation of the carbonate electrolyte translates to less formation of acidic species, the reason why no serious corrosion phenomena, such as etched surfaces and corrosion pits, are detected for AlF_3-coated material. The reduced acidic corrosion and the limited accumulation of SEI layer results in an enhancement of the structural stability of the spinel-like phase and the electrode/electrolyte interface, which further enables the reversible lithium ion intercalation/deintercalation processes in the spinel-like phase. Indeed, although the phase transformation from layered to spinel-like was still observed near the surface of the coated sample, the inert AlF_3 coating layer could alleviate or delay this unfavorable phase transformation. The valence states of the Mn/Co/Ni ions in the AlF_3-coated material after cycling are much more stable as compared to those in uncoated material. This result substantiates that the coating layer depresses the attack by acidic species and significantly reduces the formation of oxygen-deficient surfaces. In particular, the suppression of the formation of lower valence (Mn^{3+}) could largely decrease the disproportionation of Mn^{3+} in the spinel-like phase and thus promise the improved capacity retention.

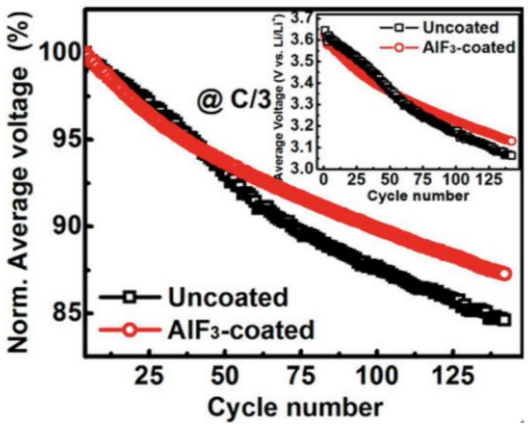

Figure 9. Normalized average discharge voltage of $Li_{1.2}Ni_{0.15}Co_{0.10}Mn_{0.55}O_2$ uncoated and AlF_3-coated materials as a function of cycle number. Inset shows the corresponding average discharge voltage. Reproduced with permission from [8]. Copyright 2014, American Chemical Society.

Pang et al. [54] modified the Li-rich $Li_{1.2}Mn_{0.54}Ni_{0.13}Co_{0.13}O_2$ powders using 5 wt% AlF_3 synthesized via a scalable solid-state reaction. The final product exhibited an Al and F co-doping core and a uniform LiF nano-coating that delivered a specific discharge capacity of 211 mAh g^{-1} after 99 cycles at 0.2C rate compared with 160 mAh g^{-1} for pristine powders. EIS results showed a 4-time increase of R_s due to the formation of resistive LiF coat, while R_{ct} is 3 times lower than that of the non-modified LNMC.

Recently, Zhao et al. [97] have prepared $LiAlF_4$- and AlF_3-coated $Li_{1.2}Ni_{0.2}Mn_{0.6}O_2$ (LNMO) cathodes and compared them. 1 wt% coating was realized by the coprecipitation method, in which

$LiNO_3$ was added as lithium source for the $LiAlF_4$ coating. The final product heated at 400 ℃ for 6 h under Ar atmosphere showed the formation of regular and stable protective layers (~5.2 nm thick). XPS measurements carried out in the binding energy range 528–536 eV showed the evolution of the O 1s peaks corresponding to the lattice O^{2-} (O $1a_a$) and non-bonding O^{n-} surface species (O $1a_b$, O $1a_c$). Upon AlF_3 coating, the O $1a_a$ peak at 529.3 eV slightly declined, while the other peaks at 531.6 and 533.3 eV, respectively, increased importantly. Rate capability performed at 5C rate demonstrated respective capacity retention of 23.9%, 40.8% and 52.4% (133 mAh g^{-1}) for LNMO, LNMO@AlF_3 and LNMO@$LiAlF_4$. The ultralong stability of LNMO@$LiAlF_4$ upon 3000 cycles is attributed to the heterostructured $LiAlF_4$ coating, in which nonbonding O^{n-} species were generated. Chen et al. [99] prepared Li-rich $Li_{1.2}Ni_{0.13}Co_{0.13}Mn_{0.53}O_2$ coated by AlF_3 (2-nm thick) by centrifugation of the precursor with the NH_4F solution and washed with ethanol. To avoid the formation of Al_2O_3, an excess of NH_4F compared with $Al(NO_3)_3$ was used, i.e., with NH_4F:$Al(NO_3)_3$ ratio of 3:1 in molar. A composite cathode was prepared by mixing Li-Rich@AlF_3 with graphene in the weight ratio of 95:5. This electrode delivered a specific capacity of ~110 mAh g^{-1} at 2C rate after 250 cycles.

3.5. AlF_3-coated NCA

As a derivative of $LiNiO_2$, $LiNi_{1-x-y}Co_xAl_yO_2$ (NCA) exhibits enhanced properties due to the presence of Co and Al [129]. Surface of NCA particles was fluorinated with NH_4F (with F:NCA ratio of 1 at%) by solid-state reaction at 300–700 ℃ for 2 h. As evidenced by XPS measurements, the surface metal–oxygen (*M*–O) bonds were partially replaced of by metal–fluorine (*M*–F) bonds. The XPS O 1s spectrum displayed a binding energy shift towards lower energies for the fluorinated NCA sample of 0.21 and 0.27 eV for the lattice oxygen (M^{3+}–O at the surface) peak at 528–530 eV and the peak due to chemically absorbed species (LiOH or Li_2CO_3) at 531–533 eV, respectively. This fluorination protects the *M*–O bonds from side reaction, reduces the release of oxygen and lowers the charge transfer resistance [99]. In the coprecipitation method, the molar ratio of F to Al was kept at 1:7 and the 0.25 mol% to the NCA powder in the solution produced a 10-nm thick coating layer [100]. Park et al. [101] deposited a uniform AlF_3 thin film of ~10 nm (0.25 mol%) on the surface of NCA powders and tested the cycle performance in the temperature range from −10 ℃ to 55 ℃. It is believed that the coating reduced the catalytic effect of Ni^{4+} and the formation of $Li_xNi_{1-x}O$-type oxide on the NCA surface operating at temperatures higher than 55 ℃. Zhang et al. [102] modified the surface of NCA particles using AlF_3 and $AlPO_4$ deposits. The cycleability of the AlF_3-coated NCA was quite stable, with a capacity retention of 96.3% of its initial after 30 cycles. A 50-nm thick AlF_3 layer was deposited on NCA particles by simple dry coating process using AlF_3 synthesized from an aqueous solution of $Al(NO_3)_3$•$9H_2O$ and NH_4F with a molar ratio of 1:7 [103]. Electrochemical tests carried out at a current density of 20 mA g^{-1} (0.1C rate) in the voltage range 2.7–4.3 V at 55 ℃ showed improved cycling behavior with ~85% capacity retention (initial capacity of 200 mAh g^{-1}). The long-term cycling performance of a full Li-ion cell with mesocarbon microbeads as anode displayed a capacity retention of 86% after 1000 cycles performed at 1C rate over the voltage range 3.0–4.2 V at room temperature. TEM bright field images of the coated electrode after 500 cycles evidenced the absence of cracks and particle pulverization. Furthermore, analysis of metal-ion dissolution by ICP for electrodes charged at 4.2 V and stored at

55 ℃ for 4 weeks showed a drastic decrease of dissolved contents of Ni and Co, i.e., 10 and 1.2 ppm, respectively, against 24 and 4.1 ppm for the pristine NCA.

3.6. AlF_3-coated spinel frameworks

It is well known that the discharge capacity of spinel $LiMn_2O_4$ suffers from irreversible capacity loss due to Mn dissolution during cycling at elevated temperatures exceeding 55 ℃ [130]. The AlF_3-coated $Li_{1.1}Mn_{1.85}Al_{0.05}O_4$ spinel-like electrode was synthesized by coprecipitation method via calcination at 400 ℃ for 5 h [104]. The 10-nm thick coated appeared to be beneficial for cycling at 55 ℃ in the range 3.0–4.3 V. A specific discharge capacity of 95 mAh g^{-1} was delivered at 5C rate compared with 90 mAh g^{-1} for the pristine material. This coated electrode sustained an excellent capacity retention of 96.2% after 100 cycles and was protected against Mn dissolution in the fully charge state (4.3 V), since after 4 weeks at 55 ℃, the dissolution was reduced to 83 ppm against 280 ppm for pristine $Li_{1.1}Mn_{1.85}Al_{0.05}O_4$. Complete blocking of Mn^{3+} dissolution from the $LiMn_2O_4$ surface can be insured by AlF_3 coating [105]. Tron et al. [106] investigated $LiMn_2O_4$ coated with 2 wt% AlF_3 as cathode material in 1 mol L^{-1} Li_2SO_4 aqueous electrolyte. A 4-Ah Li-ion battery with graphite anode and AlF_3-coated $LiMn_2O_4$ spinel cathode was investigated in the voltage range 3.0–4.2 V vs. Li^+/Li at 0.2C rate [107]. With 0.5 mol% (2.2 wt%) AlF_3, the coated $LiMn_2O_4$ powders displayed an enhanced capacity retention of 5.4% after 100 cycles. The improved performance of the AlF_3-coated $LiMn_2O_4$/graphite battery was evidenced by the storage test at 25 ℃, leading to a slight increase of the charge transfer resistance R_{ct} from 121 to 145 Ω after 28 days, while R_{ct} increased up to 386 Ω for the uncoated spinel. Wang et al. [108] fabricated sophistical Al-F codoped spherical spinel particles (15 μm size), $LiMn_{1.96}Al_{0.04}O_{3.94}F_{0.06}$, via solid-state reaction followed by 1 mol% AlF_3 coating via coprecipitation method. Due to the strong and stable Al–F bonds, the 20-nm thin layer of AlF_3 exhibited several qualities such as high ionic conductivity and chemical and electrochemical stability, which can negate the oxygen activity on the electrode surface during cycling. Therefore, AlF_3 appears to be an efficient coating material for $LiMn_2O_4$ in aqueous rechargeable lithium batteries. The best cycling behavior od the Li-rich layered-spinel structure $Li_{1.3}Mn_{4/6}Ni_{1/6}Co_{1/6}O_{2.4}$ was obtained with a AlF_3 coating of 2 wt%. The good capacity retention of 90% after 50 cycles at 0.6C rate over the voltage range 2.0–4.8 V was mainly attributed to the stable charge transfer resistance [109].

Spinel $LiNi_{0.5}Mn_{1.5}O_4$ (LNM) high-voltage cathode was modified by different amounts of AlF_3 using coprecipitation coating process [110–112]. EIS measurements on the 1 wt% AlF_3-coated LNM demonstrated the inhibition of the growth of the SEI and the prevention of Mn^{3+} dissolution in the electrolyte, resulting in improved reversibility [110]. The best cycling behavior of the Li-rich layered-spinel structure $Li_{1.3}Mn_{4/6}Ni_{1/6}Co_{1/6}O_{2.4}$ was obtained with a AlF_3 coating of 2 wt%. The good capacity retention of 90% after 50 cycles at 0.6C rate over the voltage range 2.0–4.8 V was mainly attributed to the stable charge transfer resistance [113]. Li et al. [111] reported the improved performance of $LiNi_{0.5}Mn_{1.5}O_4$ cathode material coated with various amounts of AlF_3 (1, 2 and 4 mol% of the LMN powders). 4 mol% AlF_3-coated sample exhibited a high specific capacity of 115 mAh g^{-1} at 2C rate (300 mA g^{-1}) for 40 cycles in the voltage range 3.0–4.9 V compared to 84 mAh g^{-1} for the uncoated sample. Ke et al. [112] successfully coated well-crystallized LNM powders with amount of AlF_3 up to 3 mol%. Results show that, delivering a specific capacity of 109 mAh g^{-1} at 10C rate, this cathode is suitable for high-power batteries for electric vehicles.

3.7. Other cathodes coated with AlF_3

The surface of the olivine-type $LiFePO_4$ (LFP) electrode was partly modified by a coating of nano-sized AlF_3 and Al_2O_3 deposits, which appeared to be interfacial stabilizer by improvement of the overall electrochemical behaviors [113]. Song et al. [114] examined the influence of AlF_3 nano-coating (nominal 2 wt%) on the electrochemical behaviors of LFP cathode at 60 ℃ in Li-ion battery including graphite as anode. The 5-nm thick coating maintains a specific capacity of 130 mAh g^{-1} at 1C rate after 100 cycles over 2.2–3.8 V vs. Li^+/Li (capacity retention of 92%). Tron et al. [115] prepared an LFP electrode coated with 1 wt% AlF_3 deposit via coprecipitation method. This material used as a cathode in an aqueous rechargeable lithium battery with 1 mol L^{-1} Li_2SO_4 dissolved in water as electrolyte delivered a specific capacity of 132 mAh g^{-1} at 1C rate and a capacity retention of 93% after 100 cycles. Electrochemical properties of optimized 4 mol% AlF_3-coated $LiCoPO_4$ olivine-like cathode indicated improved cycleability and rate capability with initial discharge capacity of 159 mAh g^{-1} at C/10 rate and 91% capacity retention over 50 cycles [116]. AlF_3 coating of $Li_3V_2(PO_4)_3$/C composite material was prepared via a conventional precipitation method. The capacity retention rate of LVP/C-AlF_3 was 85% after 50 charge/discharge cycles at 0.2C rate in the voltage range 3.0–4.8 V that compared to 76% of the uncoated material [131].

LiV_3O_8 (LVO) with monoclinic structure was considered for use in lithium polymer batteries (LPBs) [132]. A 2.9 wt% AlF_3-coated LVO prepared by conventional coprecipitation method was formed as core-shell particle with an intermediate $Li_xV_2O_5$ thin layer. It was suggested that NH_4F in the coating precursor reacts with LiV_3O_8 during calcination [133]. Cycling performance was investigated at a current density of 150 mA g^{-1} in the voltage range 1.8–3.8 V. The AlF_3-coated LVO demonstrated an initial capacity of 231 mAh g^{-1} and a capacity retention of 91.8% over 50 cycles. It was suggested that the AlF_3 layer prevents the capacity loss due to the incomplete reversibility of the transformation between $Li_4V_3O_8$ and LiV_3O_8 phases and better retains the discharge voltage plateaus.

4. Characterization of the coating/electrode interface

4.1. Raman spectroscopy

Generally, the XRD pattern of AlF_3-coated electrode does not display any trace of Al-F compound because the deposited coat is a thin amorphous phase. The non-destructive Raman spectroscopy is a powerful analytical method to probe the surface of coating layers compared to XRD technique especially in the case of highly disordered or amorphous materials [134]. It is also used to study the environment of lithium ions in lithiated metal oxides because the internal modes of LiO_6 occur in the spectral range 200–300 cm^{-1}, while those of LiO_4 appear in the range 350–500 cm^{-1} [135,136]. The Raman spectrum of α-AlF_3 displays four fundamental active vibrations including external (in the low-frequency range) and internal modes. In the Mulliken notation of the D_{3d} symmetry, they decompose in $1A_{1g} + 3E_g$ among which E_g modes are doubly degenerate. The rotation mode of AlF_6 octahedra (E_g) is located at 96 cm^{-1}, the A_{1g} rotation mode of AlF_6 at 157 cm^{-1}, the E_g bending mode of Al–F–Al bonds at 382 cm^{-1} and the E_g stretching vibration of Al–F bonds at 478 cm^{-1} [137]. Note that the external modes have a strong intensity, while internal modes are very weak in the ratio 1:25. For this reason, the external Raman bands of the AlF_3 coating are solely

observed as shown in Figure 10. Due to the lower symmetry and inequivalent atomic positions in the elementary unit cell of β-AlF_3, the larger number of Raman active modes is classified as $8A_g + 7B_{1g} + 7B_{2g} + 5B_{3g}$. Experimental Raman data display only two spectral features located at 75 (strong) and 411 cm^{-1} (moderate) assigned to rotational mode of AlF_6 (A_g), and the bending mode of Al–F–Al bonds (A_g), respectively [138].

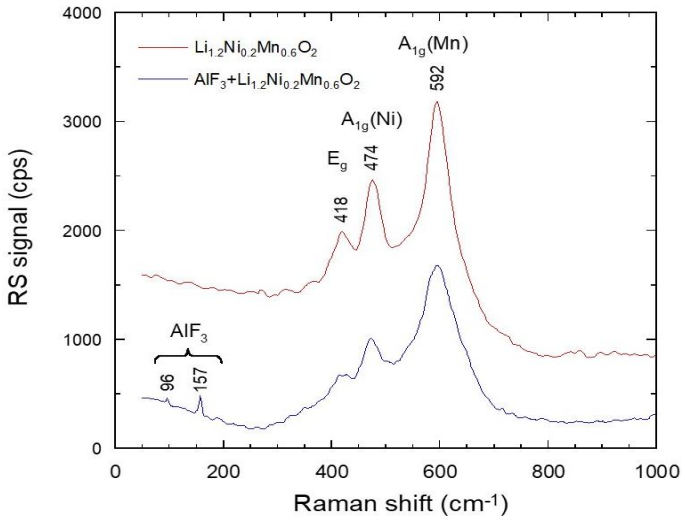

Figure 10. Raman spectra of Li-rich cathode materials (a) pristine and (b) $Li_{1.2}Ni_{0.2}Mn_{0.6}O_2$ coated with a thick AlF_3 layer (~40 nm). Raman bands of rotational modes of AlF_6 are observed in the low-frequency range.

4.2. X-ray photoelectron spectroscopy

X-ray photoelectron spectroscopy (XPS) is currently used as analytical tool to determine the composition and the sputter depth profile of AlF_3 films [50]. Makarowicz et al. [139] distinguished the local geometric structure of α- and β-AlF_3 surfaces using XPS with surface Al^{3+} sites contributing to the Al 2p binding energy peak at 77.1 and 76.1 eV, respectively. The binding energy of F 1s was reported to be 686.7 eV in α-AlF_3, which deviates to 686.7 eV in β-AlF_3. Table 2 lists the Li 1s, Al 2p and F 1s XPS data for LiF, $LiAlF_4$ and AlF_3 ALD films. Note that the F 1s peak in AlF_3 and $LiAlF_4$ are shifted to higher binding energy compared to that in LiF due to the higher electronegativity of Al compared to Li. In the F 1s XPS spectrum, the band appearing at 687.3 eV is attributed to the C–F bonds of the PVdF binder [130].

Table 2. The Li 1s, Al 2p and F 1s XPS data for LiF, $LiAlF_4$ and AlF_3 ALD films. Reproduced with permission from [66]. Copyright 2017, American Chemical Society.

Element	Binding energy (eV)		
	LiF	$LiAlF_4$	AlF_3
Li 1s	55.3	55.6	-
Al 2p	-	75.3	76.2
F 1s	684.8	685.5	686.5

4.3. Electrochemical impedance spectroscopy

One of the most powerful tools to characterize the evolution of the electrical and electrochemical properties of a battery electrode is the electrochemical impedance spectroscopy (EIS), which can reveal the improved performance of an electrochemical system. EIS is widely used to analyze the kinetics of electrode reaction and the effect of EEI on kinetics [140]. A Nyquist plot, i.e., $Z'(\omega)$ vs. $Z''(\omega)$, is the response of a sample or a cell excited by an a.c. signal analyzed in terms of complex impedance $Z(\omega) = Z'(\omega) + jZ''(\omega)$ (or admittance $Y(\omega) = Y'(\omega) + jY''(\omega)$) in a wide frequency range from 10 MHz to 0.01 Hz [141]. EIS experiments are a good tool to detect the improvement of protective coatings using adequate equivalent circuits. An equivalent circuit that describes the spectrum is not unique but a good fit to the experimental data must represent an accurate physical model of the studied system [142]. Experimentally, four regions can be distinguished in an EIS spectrum: (i) the intercepts with the Z' axis at high frequency is related to the ohmic resistance of the cell (R_Ω), (ii) the semicircle at high frequency corresponds to the passivating SEI surface film and coating layer (R_S), (iii) the intermediate-frequency semicircle is related to the charge transfer resistance R_{ct} at the electrode/electrolyte interface and (iv) the low-frequency range is ascribed to the ion diffusion process in the bulk electrode, i.e., designed as Warburg component. Thus, the real part of the total impedance is described by:

$$Z' = R_\Omega + R_S + R_{ct} + \sigma_w \omega^{-1/2}, \quad (12)$$

where ω is the frequency and σ_w is the Warburg factor. The linear fit of Z' vs. $\omega^{-1/2}$ plot provides the values of the Warburg impedance factor.

Generally, EIS results are attributed to the fact that, during the charging and discharging process, the coating layer can suppress the increase of impedance by impeding a direct contact between the highly delithiated electrode and the electrolyte, thus reducing the charge transfer resistance, R_{ct}. Several reports have shown the efficiency of in situ EIS experiments. Zheng et al. [143] have drawn considerable attention on the cycling performance at relatively high rate for Li- and Mn-rich layered electrodes. They reported the improved electrochemical performance of the AlF_3-coated $Li[Li_{0.12}Mn_{0.54}Ni_{0.13}Co_{0.13}]O_2$ electrode, i.e., capacity retention of 87.9% against 67.8% for pristine material after 80 cycles at C/2 rate, and the better thermal stability as well. The "buffer" layer effect provided by the AlF_3 deposit analyzed by electrochemical impedance spectroscopy (EIS) and in situ differential electrochemical mass spectrometry (DEMS) was tentatively attributed to the stabilization of the electrode/electrolyte interface by reduction of the active extracted oxygen and suppression of the electrolyte decomposition at voltages < 4.5 V vs. Li^+/Li. Figure 11 presents the variation of the charge-transfer resistance, R_{ct}, as a function of number of cycles for pristine and AlF_3-coated $Li[Li_{0.2}Mn_{0.54}Ni_{0.13}Co_{0.13}]O_2$. R_{ct} of pristine material increases faster than that of the AlF_3-coated electrode upon cycling. DEMS experiments demonstrated that AlF_3 coating prevents O_2 evolution during potential scan: leakage of O_2 occurs at a voltage of 4.30 V in the pristine material, while it starts at 4.75 V for the coated electrode, beyond the oxidation of Co^{3+}–Co^{4+}. Sun et al. [70] reported a lower R_{ct} and reduced cobalt dissolution in AlF_3-coated $LiCoO_2$ charged at the cutoff voltage of 4.5 V. Using a 10 nm-thick AlF_3 layer, R_{ct} was maintained at 20–27 Ω during cycling. On the other hand, R_{ct} rapidly increased from 74 to 2044 Ω at the 50th cycle for pristine $LiCoO_2$, due to the formation of a SEI film composed of alkyl carbonate, LiF, Li_xPF_y and $Li_xPF_yO_z$ compounds. R_{ct} is a function of several parameters: the amount of AlF_3 coating, i.e., the film thickness, but also the

uniformity and the mesoporosity of the deposit. The same group of workers showed enhanced electrochemical performance associated with stable charge transfer resistance, which in turn limited the increase of the total cell resistance in AlF_3-coated $LiNi_{1/3}Co_{1/3}Mn_{1/3}O_2$ [28].

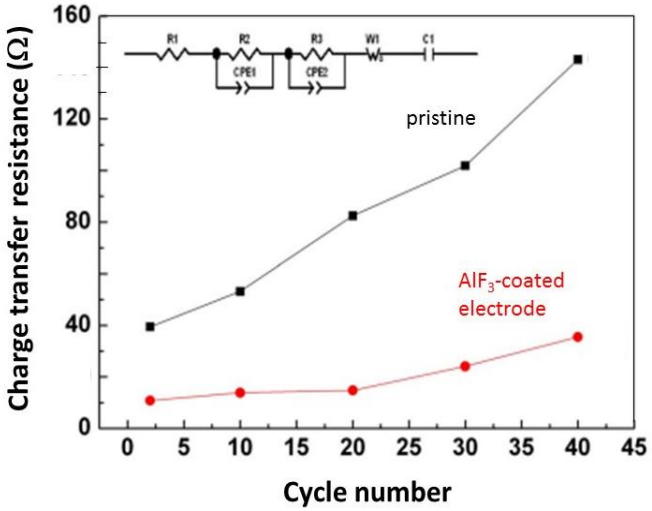

Figure 11. Evolution of the charge-transfer resistance, R_{ct}, as a function of cycle life for pristine and AlF_3-coated $Li[Li_{0.2}Mn_{0.54}Ni_{0.13}Co_{0.13}]O_2$. Electrodes were cycled at 0.5C rate over the voltage range 2.0–4.8 V. Reproduced with permission from [143]. Copyright 2008, The Electrochemical Society.

During long life cycling, an abrupt increase in charge-transfer resistance of the cathode is currently observed and it is considered as the main reason for capacity fading [144]. Enhancement of the stability of the interfacial resistance between the cathode and the electrolyte has been widely demonstrated by EIS. One reason for the stable cathode/electrolyte interface after AlF_3 coating is its strong resistance to HF, so that AlF_3 act as a stabilizer protecting the oxide structure from damage. Using a time-of-flight-secondary ion mass spectroscopy (ToF-SIMS), Myung et al. [10] showed that the coating layer works also as HF scavenger.

4.4. Area-specific impedance

Because of the different combined factors that change the overall cell potential, the basic concept of the area-specific impedance (ASI, expressed in $\Omega\ cm^2$) is an efficient test for the performance of a lithium-insertion electrode. ASI is determined from the change in the equilibrium potential as a function of the depth of discharge (DOD) after pulse of current for a given passed charge by the relation [145–150]:

$$ASI = A\frac{OCV - V_{cell}}{I}, \tag{13}$$

where A is the cross-sectional area of the electrode and I is the current passed throughout the cell. $\Delta V = OCV - V_{cell}$ is the potential change during current interruption for 60 s at each DOD step. Belharouak et al. [147] reported an ASI of 50 $\Omega\ cm^2$ for a NMC333 electrode subjected to a pulse of

18 s. The $LiCoO_2$ coating (~20 nm thick) of $Li_{1.05}Ni_{0.35}Co_{0.25}Mn_{0.4}O_2$ highly improved the ASI value (38 Ω ċm^2 against 55 Ω ċm^2 measured for a cathode discharged at 90% DOD when cycled between 2.8–4.5 V) [148]. These results show that, during battery charging, the charge-transfer resistance is dependent of DOD. Note that ASI can be described in terms of cell polarization and power dissipation generating heat [151]. Figure 12 presents the variation of ASI vs. DOD of AlF_3-coated $LiNi_{0.5}Mn_{0.5}O_2$ as a function of the coating concentration. These results show that the lower ASI value is obtained for AlF_3-coating of 4%, which is beneficial for the long-life cycling behavior. Similar results have been reported for AlF_3-coated $Li_{1.2}Ni_{0.2}Mn_{0.6}O_2$ electrode. For 90% DOD, the ASI decreased from 37 to 30 Ω ċm^2 for the coated material [74].

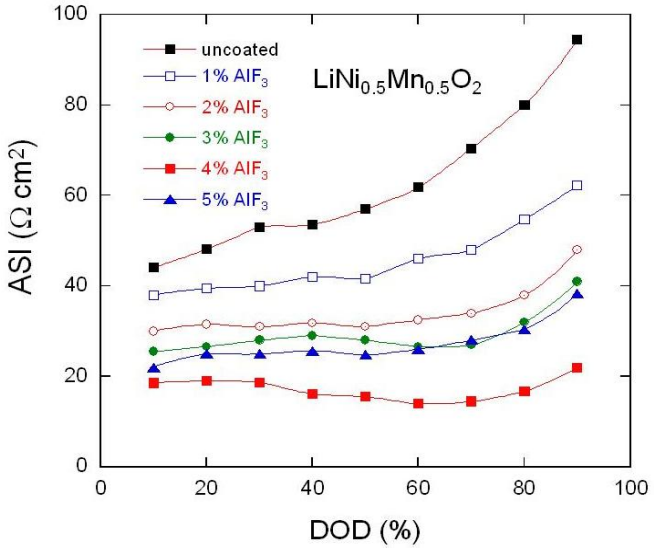

Figure 12. Depth of discharge (DOD) dependence of the area-specific impedance (ASI) of AlF_3-coated $LiNi_{0.5}Mn_{0.5}O_2$ as a function of the coating concentration.

4.5. Thermal stability

Safety of lithium batteries is one of the main concerns associated to the risk of thermal runaway and battery fire [152]. The thermal stability is currently investigated by differential scanning calorimetry (DSC). As an example, Figure 13 shows that the $Li[Li_{0.2}Mn_{0.54}Ni_{0.13}Co_{0.13}]O_2$ electrode is unsafe when at charged state to 4.8 V (delithiated state). The DSC profile of the pristine material exhibits the onset temperature of thermal decomposition from at 206.6 ℃ with an associated exothermic heat of 924 J g^{-1}, which is greatly reduced to 538 J g^{-1} for the AlF_3-coated electrode. Also, the thermal decomposition increased to 223.8 ℃ in the surface-modified layered material [143].

To avoid their individual electrochemical drawbacks $LiCoO_2$ and $LiNi_{1/3}Mn_{1/3}Co_{1/3}O_2$ were associated to form an AlF_3-coated (LCO/NMC) blended cathode material [78]. The specific discharge capacity for the blended electrodes was found to be in the range 180–188 mAh g^{-1} at a current density of 90 mA g^{-1} (0.5C rate) in the electrochemical window 3.0–4.5 V vs. Li^+/Li, depending on the blend ratio, the best composition being LCO:NMC of 7:3.

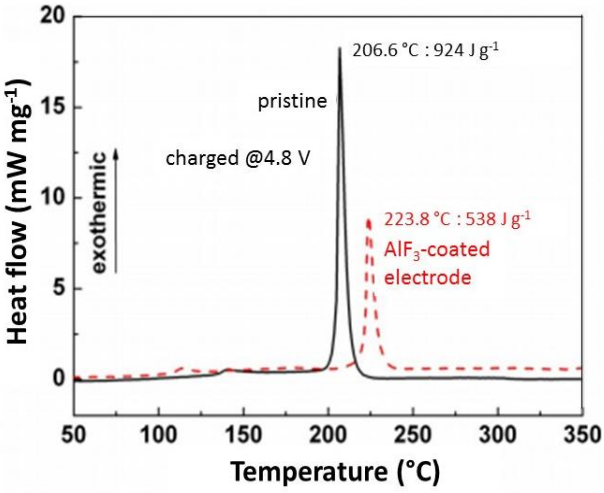

Figure 13. DSC profiles of pristine and AlF_3-coated $Li[Li_{0.2}Mn_{0.54}Ni_{0.13}Co_{0.13}]O_2$ electrodes charges at 4.8 V vs. Li^+/Li. The heat produced during thermal decomposition is reported for each onset temperature. Reproduced with permission from [143]. Copyright 2008, The Electrochemical Society.

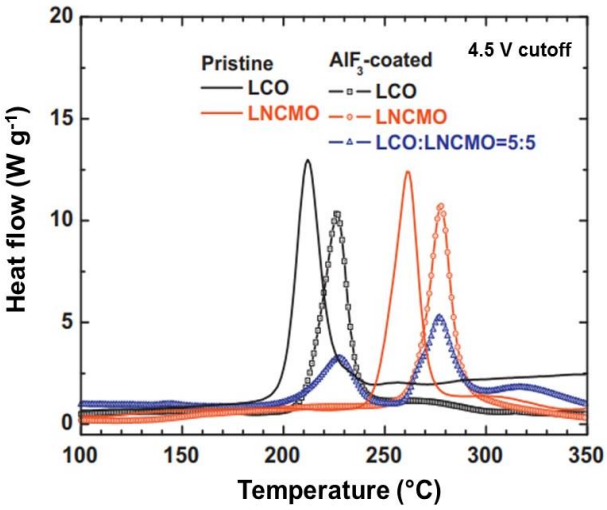

Figure 14. The effect of AlF_3 coating on the thermal stability of blended $LiCoO_2/LiNi_{1/3}Mn_{1/3}Co_{1/3}O_2$ electrodes in the charge state, i.e., at potential of ~4.5 V vs. Li^+/Li. Reproduced with permission from [78]. Copyright 2011, Elsevier.

Figure 14 shows the effect of AlF_3 coating on the thermal stability of blended LCO/NMC electrodes in the charge state, i.e., at potential of ~4.5 V vs. Li^+/Li. For pristine $LiCoO_2$ and $LiNi_{1/3}Co_{1/3}Mn_{1/3}O_2$ electrodes, the DSC curves exhibit an exothermic peak at 212 and 261 ℃, which generated an exothermic heat of 2785 and 1998 J g^{-1}, respectively. For both AlF_3-coated materials, the exothermic peak shifts toward high temperatures and the resulting heat is reduced. Meanwhile, the better thermal stability of the NMC333 powders is attributed to the electrochemically inactive tetravalent Mn in the layered lattice. The DSC curve of the LCO/NMC blend electrode demonstrates

the smaller exothermic peaks at 227 and 277 ℃ with a total lower generated heat of 1665 $J \cdot g^{-1}$. It is assumed that the insulating AlF_3 layer suppresses the oxygen release from the blended particles.

The cycle performance of typical AlF_3-coated cathode materials is summarized in Table 3. Although for many electrodes the intrinsic properties of the AlF_3 coating are not provided, several remarks can be made in relation with the electrochemical performances of positive electrodes for LIBs. Until then, the electrodes with layered structure (LCO, NCA, NMC and Li-rich NMC) have been the most studied to increase the capacity retention. Some spectacular results deserve to be mentioned.

Table 3. The beneficial effects of AlF_3 coating on the cycle performance of typical cathode materials.

Electrode material	Deposit amount	Thickness (nm)	Specific capacity ($mAh\ g^{-1}$)		Rate/cycles	Ref.
			pristine	coated		
$LiCoO_2$	0.5 mol%	5–10	110	182	C/2 (50)	[28]
$LiCoO_2$	2 mol%	10	30	170	C/5 (50)	[67]
$LiCoO_2$	2 mol%	10	110	175	C/2 (50)	[71]
$LiCoO_2$	2 mol%	10–15	110	150	C/5 (17)	[72]
$LiNi_{0.8}Co_{0.15}Al_{0.05}O_2$	¼ mol%	10	155	180	0.5C (50)	[100]
$LiNi_{0.8}Co_{0.15}Al_{0.05}O_2$	1 wt%	50	66.5	86.2	1C (1000)@25 ℃	[103]
$LiNi_{1/3}Mn_{1/3}Co_{1/3}O_2$	1.5 wt%	3	64	120	2C (80)	[76]
$LiNi_{1/3}Mn_{1/3}Co_{1/3}O_2$	¼ mol%	10	-	172	0.5C (50)@30 ℃	[78]
Blended LCO:NMC333 (7:3)	¼ mol%	10	-	180	0.5C (50)@30 ℃	[78]
$LiNi_{1/3}Mn_{1/3}Co_{1/3}O_2$	¼ mol%	10	150	170	0.2C (50)	[79]
$LiNi_{0.5}Co_{0.2}Mn_{0.3}O_2$	0.5 mol%	-	155	170	1C (50)@55 ℃	[85]
$LiMn_2O_4$	2 wt%	-	80	92	1C (100)	[107]
$Li_{1.1}Mn_{1.85}Al_{0.05}O_2$	-	10–15	85	105	C/2 (100)	[104]
$LiMn_{1.96}Al_{0.04}O_{3.94}F_{0.06}$	1 mol%	20	105	108	C/5 (100)	[153]
$LiNi_{0.8}Co_{0.15}Al_{0.05}O_2$	1 wt%	50	155	170	C/2 (100)@55 ℃	[99]
$Li_{1.2}Ni_{0.15}Co_{0.1}Mn_{0.55}O_2$	1 wt%	10	169	210	C/3 (150)	[8]
$Li_{1.19}Ni_{0.16}Co_{0.08}Mn_{0.57}O_2$	2 wt%	-	165	175	0.5C (100)	[45]
$Li_{1.2}Mn_{0.54}Ni_{0.16}Co_{0.08}O_2$	0.5 vol%	5–7	100	150	1C (50)	[91]
$Li_{1.24}Ni_{0.12}Co_{0.12}Mn_{0.56}O_2$	2 wt%	2	<120	220	0.1C (50)@55 ℃	[92]
$Li(Li_{0.17}Ni_{0.25}Mn_{0.58})O_2$	2 wt%	5–7	<25	104	5C (200)	[87]
$LiFePO_4$	1 wt%	-	123	132	1C (100)	[115]
$LiCoPO_4$	4 mol%	4	110	159	0.1C (50)	[116]
LiV_3O_8	5 wt%	-	61	91	0.5C (50)	[133]
LiV_3O_8	1 wt%	-	25	70	1C (50)	[154]
$Li_4Ti_5O_{12}$	10 wt%	100–200	120	130	1C (260)	[116]

The beneficial effect of AlF_3 coating on $LiCoO_2$ particles is twofold. First, an extended charge cut-off voltage from 4.2 to above 4.5 V vs. Li^+/Li allows a large enhancement of the practical specific capacity due to the surface preservation of the deposit against nucleation of irreversible cubic spinel phase. Using a 10-nm thick AlF_3 deposit (2 mol%), the best performance of LCO powders is an initial specific capacity of 210 mAh g^{-1}, which is retained at 190 mAh g^{-1} after 50 cycles at 0.5C rate [72]. Second, the amount of Co dissolution of the electrode charged at 4.5 V is limited to 18 ppm over 6 weeks. An interesting analysis of the microstructural properties versus AlF_3 content for coated $LiNi_{0.5}Co_{0.2}Mn_{0.3}O_2$ shows that the XRD peak ratio I_{003}/I_{104} is optimum for a coating of 0.5 mol% corresponding to the minimum Li/Ni cation mixing [85], which improves significantly the electrochemical performance due to the better Li^+ ion diffusion. So, this material is a good candidate for electric vehicle power batteries. Similar situation was reported for AlF_3-coated $LiNi_{1/3}Mn_{1/3}Co_{1/3}O_2$, for which a 10-nm thick AlF_3 layer deposited by the aqueous coprecipitation process remarkably enhances the capacity retention to 96% after 50 charge–discharge cycles at 0.5C rate [79]. As discussed before, the nanoscaled AlF_3 layer must be amorphous and homogeneous that are features obtained at a low-temperature annealing of about 400 ℃ [77].

One of the best results obtained so far, is from the 50-nm AlF_3 coated $LiNi_{0.8}Co_{0.15}Al_{0.05}O_2$ [104]. At 25 ℃, this electrode delivered 86.2% of its initial capacity over 1000 cycles at 1C rate (current density of 190 mA g^{-1}) against 66.5% for the pristine materials. When tested under the high-temperature regime at 55 ℃, AlF_3-coated NCA exhibited a capacity retention of 55.9%, which is almost 5 times that of the pristine NCA electrode. Concerning the new generation of cathode materials, i.e., Li-rich NMCs, the recent work by Amalraj et al. [86] reports that $xLi_2MnO_3\bullet(1-x)Li[Mn_yNi_zCo_w]O_2$ electrodes coated with extremely small AlF_3 nanocrystals (5–8 nm in size, tetragonal *P*4*nmm* symmetry) exhibit a capacity fade of 25% over 200 cycles at C/5 rate and demonstrate a high Li storage capability at 60 ℃. The authors suggest that conductive species such as $Li_{1-x}AlF_{3+x}$ and Al[FOH] are formed during the first charge process that promote the low-resistive electrode–electrolyte interface. Finally, note that several authors have investigated the electrochemical performance of AlF_3-coated electrode at temperature of 55 ℃, which is the critical test for checking the material stability [85,92,99].

5. Conclusions

In this paper we have examined the beneficial effect of aluminum fluoride nano-coatings on electrochemical properties of positive electrode materials for Li-ion batteries. The role of nanoscale surface modification of cathode materials for Li-ion batteries has shown that the coating increases the energy density, improves the calendar and cycling life and enhances the thermal stability. AlF_3 is thought to be a standout amongst the most promising coating materials for the improvement in thermal stability as well as electrochemical performances, because AlF_3 can form more stable coating layer than oxides and supports faster Li^+ deintercalation/intercalation. Deposition of AlF_3 thin layer is very easy using the popular coprecipitation method. Recently, a more sophisticated synthesis such as ALD has been used. It is believed that fast-ionic conducting solid layer $LiAlF_4$ can be created that favors the Li^+-ion transport throughout the electrode/electrolyte interface. The excellent efficiency of the AlF_3 coating is highlighted for the Li-rich layered NMC oxides, which can deliver a high specific capacity superior to 250 mAh g^{-1} at moderate C-rate. Therefore, a comparison of the electrochemical performance is difficult because the particle size distribution is rarely

documented. Among the specific characterization methods Raman spectroscopy, electrochemical impedance spectroscopy and differential capacity have probed the stabilization of the host structure and the electrode/electrolyte interface.

Conflict of interest

There is no conflict of interest related to this document.

References

1. Julien CM, Mauger A, Vijh A, et al. (2016) *Lithium Batteries*, Switzerland: Springer, Cham.
2. Vetter J, Novák P, Wagner MR, et al. (2005) Ageing mechanisms in lithium-ion batteries. *J Power Sources* 147: 269–281.
3. Tröltzsch U, Kanoun O, Tränkler HR (2006) Characterizing aging effects of lithium ion batteries by impedance spectroscopy. *Electrochim Acta* 51: 1664–1672.
4. Kiziltas-Yavuz N, Herklotz M, Hashem AM, et al. (2013) Synthesis, structural, magnetic and electrochemical properties of $LiNi_{1/3}Mn_{1/3}Co_{1/3}O_2$ prepared by a sol-gel method using table sugar as chelating agent. *Electrochim Acta* 113: 313–321.
5. Birkl CR, Roberts MR, McTurk E, et al. (2017) Degradation diagnostics for lithium ion cells. *J Power Sources* 341: 373–386.
6. Cabana J, Kwon BJ, Hu L (2018) Mechanisms of degradation and strategies for the stabilization of cathode–electrolyte interfaces in Li-ion batteries. *Accounts Chem Res* 51: 299–308.
7. Xu Z, Rahman MM, Mu L, et al. (2018) Chemomechanical behaviors of layered cathode materials in alkali metal ion batteries. *J Mater Chem A* 6: 21859–21884.
8. Zheng JM, Gu M, Xiao J, et al. (2014) Functioning mechanism of AlF_3 coating on the Li- and Mn-rich cathode materials. *Chem Mater* 26: 6320–6327.
9. Tasaki K, Kanda K, Nakamura S, et al. (2003) Decomposition of $LiPF_6$ and stability of PF_5 in Li-ion battery electrolytes. *J Electrochem Soc* 150: A1628–A1636.
10. Myung ST, Izumi K, Komaba S, et al. (2005) Role of alumina coating on Li-Ni-Co-Mn-O particles as positive electrode material for lithium-ion batteries. *Chem Mater* 17: 3695–3704.
11. Chen Z, Qin Y, Amine K, et al. (2010) Role of surface coating on cathode materials for lithium-ion batteries. *J Mater Chem* 20: 7606–7612.
12. Mauger A, Julien CM (2014) Surface modifications of electrode materials for lithium-ion batteries: status and trends. *Ionics* 20: 751–787.
13. Jin X, Xu Q, Liu H, et al. (2014) Excellent rate capability of Mg doped $Li[Li_{0.2}Ni_{0.13}Co_{0.13}Mn_{0.54}]O_2$ cathode material for lithium-ion battery. *Electrochim Acta* 136: 19–26.
14. Zheng J, Wu X, Yang Y (2013) Improved electrochemical performance of $Li[Li_{0.2}Mn_{0.54}Ni_{0.13}Co_{0.13}]O_2$ cathode material by fluorine incorporation. *Electrochim Acta* 105: 200–208.
15. Zhang SS (2006) A review on electrolyte additives for lithium-ion batteries. *J Power Sources* 162: 1379–1394.

16. Li M, Zhou Y, Wu X, et al. (2018) The combined effect of CaF_2 coating and La-doping on electrochemical performance of layered lithium-rich cathode material. *Electrochim Acta* 275: 18–24.
17. Lu Y, Shi S, Yang F, et al. (2018) Mo-doping for improving the ZrF_4 coated-$Li[Li_{0.2}Mn_{0.54}Ni_{0.13}Co_{0.13}]O_2$ as high performance cathode materials in lithium-ion batteries. *J Alloy Compd* 767: 23–33.
18. Hashem AMA, Abdel-Ghany AE, Eid AE, et al. (2011) Study of the surface modification of $LiNi_{1/3}Co_{1/3}Mn_{1/3}O_2$ cathode material for lithium ion battery. *J Power Sources* 196: 8632–8637.
19. Yang ZX, Qiao QD, Yang WS (2011) Improvement of structural and electrochemical properties of commercial $LiCoO_2$ by coating with LaF_3. *Electrochim Acta* 56: 4791–4796.
20. Sun SH, Kim SB, Park YJ (2009) The effects of LaF_3 coating on the electrochemical property of $Li[Ni_{0.3}Co_{0.4}Mn_{0.3}]O_2$ cathode material. *B Korean Chem Soc* 30: 2584–2588.
21. Xie QL, Hu ZB, Zhao CH, et al. (2015) LaF_3-coated $Li[Li_{0.2}Mn_{0.56}Ni_{0.16}Co_{0.08}]O_2$ as cathode material with improved electrochemical performance for lithium ion batteries. *RSC Adv* 5: 50859–50864.
22. Lee HJ, Park YJ (2013) Interface characterization of MgF_2-coated $LiCoO_2$ thin films. *Solid State Ionics* 230: 86–91.
23. Shi SJ, Tu JP, Mai YJ, et al. (2012) Structure and electrochemical performance of CaF_2 coated $LiMn_{1/3}Ni_{1/3}Co_{1/3}O_2$ cathode material for Li-ion batteries. *Electrochim Acta* 83: 105–112.
24. Liu X, Liu J, Huang T, et al. (2013) CaF_2-coated $Li_{1.2}Mn_{0.54}Ni_{0.13}Co_{0.13}O_2$ as cathode materials for Li-ion batteries. *Electrochim Acta* 109: 52–58.
25. Zhang X, Yang Y, Sun S, et al. (2016) Multifunctional ZrF_4 nanocoating for improving lithium storage performances in layered $Li[Li_{0.2}Ni_{0.17}Co_{0.07}Mn_{0.56}]O_2$. *Solid State Ionics* 284: 7–13.
26. Li JG, Wang L, Zhang Q, et al. (2009) Electrochemical performance of SrF_2-coated $LiMn_{1/3}Ni_{1/3}Co_{1/3}O_2$ cathode materials for Li-ion batteries. *J Power Sources* 190: 149–153.
27. Liu BL, Zhang Z, Wan J, et al. (2017) Improved electrochemical properties of YF_3-coated $Li_{1.2}Mn_{0.54}Ni_{0.13}Co_{0.13}O_2$ as cathode for Li-ion batteries. *Ionics* 23: 1365–1374.
28. Sun YK, Cho SW, Myung ST, et al. (2007) Effect of AlF_3 coating amount on high voltage cycling performance of $LiCoO_2$. *Electrochim Acta* 53: 1013–1019.
29. Wang Z, Wang Z, Guo H, et al. (2014) Enhanced high-voltage electrochemical performance of $LiCoO_2$ coated with ZrO_xF_y. *Mater Lett* 123: 93–96.
30. Lee KS, Myung ST, Amine K, et al. (2009) Dual functioned BiOF-coated $Li[Li_{0.1}Al_{0.05}Mn_{1.85}]O_4$ for lithium batteries. *J Mater Chem* 19: 1995–2005.
31. Hao Y, Yand F, Luo D, et al. (2018) Improved electrochemical performances of yttrium oxyfluoride-coated $Li[Li_{0.2}Mn_{0.54}Ni_{0.13}Co_{0.13}]O_2$ for lithium ion batteries. *J Energy Chem* 27: 1239–1246.
32. Bai Y, Jiang K, Sun S, et al. (2014) Performance improvement of $LiCoO_2$ by MgF_2 surface modification and mechanism exploration. *Electrochim Acta* 134: 347–354.
33. Shi SJ, Tu JP, Tang YY, et al. (2013) Enhanced electrochemical performance of LiF-modified $LiMn_{1/3}Ni_{1/3}Co_{1/3}O_2$ cathode materials for Li-ion batteries. *J Power Sources* 225: 338–346.
34. Chen Q, Wang Y, Zhang T, et al. (2012) Electrochemical performance of LaF_3-coated $LiMn_2O_4$ cathode materials for lithium ion batteries. *Electrochim Acta* 83: 65–72.
35. Amatucci GG, Pereira N (2007) Fluoride based electrode materials for advanced energy storage devices. *J Fluorine Chem* 128: 243–262.

36. Cabana J, Monconduit L, Larcher D, et al. (2010) Beyond intercalation-based Li-ion batteries: The state of the art and challenges of electrode materials reacting through conversion reactions. *Adv Mater* 22: E170–E192.
37. Badway F, Cosandey F, Pereira N, et al. (2003) Carbon metal fluoride nanocomposites: High-capacity reversible metal fluoride conversion materials as rechargeable positive electrodes for Li batteries. *J Electrochem Soc* 150: A1318–A1327.
38. Bervas M, Badway F, Klein LC, et al. (2005) Bismuth fluoride nanocomposite as a positive electrode material for rechargeable lithium batteries. *Electrochem Solid-State Lett* 8: A179–A183.
39. Owen N, Zhang Q (2017) Investigations of aluminum fluoride as a new cathode material for lithium-ion batteries. *J Appl Electrochem* 47: 417–431.
40. Le Bail A, Calvayrac F (2006) Hypothetical AlF_3 crystal structures. *J Solid State Chem* 179: 3159–3166.
41. Navarro JL, Albanesi E, Vidal RA, et al. (2016) A study on the structural, electronic and optical properties of the α-AlF_3 compound. *Mater Res Bull* 83: 615–622.
42. Bridou F, Cuniot-Ponsard M, Desvignes JM, et al. (2010) Experimental determination of optical constants of MgF_2 and AlF_3 thin films in the vacuum ultra-violet wavelength region (60–124 nm), and its application to optical designs. *Opt Commun* 283: 1351–1358.
43. Myung ST, Lee KS, Yoon CS, et al. (2010) Effect of AlF_3 coating on thermal behavior of chemically delithiated $Li_{0.35}[Ni_{1/3}Co_{1/3}Mn_{1/3}]O_2$. *J Phys Chem C* 114: 4710–4718.
44. Kemnitz E, Menz DH (1998) Fluorinated metal oxides and metal fluorides as heterogeneous catalysts. *Prog Solid State Ch* 26: 97–153.
45. Sun YK, Lee MJ, Yoon CS, et al. (2012) The role of AlF_3 coatings in improving electrochemical cycling of Li-enriched nickel-manganese oxide electrodes for Li-ion batteries. *Adv Mater* 24: 1192–1196.
46. Kanamura K, Okagawa T, Takehara ZI (1995) Electrochemical oxidation of propylene carbonate (containing various salts) on aluminum electrodes. *J Power Sources* 57: 119–123.
47. Morita M, Shibata T, Yoshimoto N, et al. (2002) Anodic behavior of aluminum in organic solutions with different electrolytic salts for lithium ion batteries. *Electrochim Acta* 47: 2787–2793.
48. Ma T, Xu GL, Li Y, et al. (2017) Revisiting the corrosion of the aluminum current collector in lithium-ion batteries. *J Phys Chem Lett* 8: 1072–1077.
49. Kawamura T, Tanaka T, Egashira M, et al. (2005) Methyl difluoroacetate inhibits corrosion of aluminum cathode current collector for lithium ion cells. *Electrochem Solid-State Lett* 8: A459–A463.
50. Hennessy J, Jewell AD, Balasubramanian K, et al. (2016) Ultraviolet optical properties of aluminum fluoride thin films deposited by atomic layer deposition. *J Vac Sci Technol A* 34: 01A120.
51. Lee Y, DuMont JW, Cavanagh AS, et al. (2015) Atomic layer deposition of AlF_3 using trimethylaluminum and hydrogen fluoride. *J Phys Chem C* 119: 14185–14194.
52. Mane AU, Elam JW, Park JS, et al. (2016) Metal fluoride passivation coatings prepared by atomic layer deposition on $LiCoO_2$ for Li-ion batteries. US Patent 2016/0260962A1.

53. Zhou Y, Lee Y, Sun H, et al. (2017) Coating solution for high-voltage cathode: AlF_3 atomic layer deposition for freestanding $LiCoO_2$ electrodes with high energy density and excellent flexibility. *ACS Appl Mater Inter* 9: 9614–9619.
54. Pang S, Wang Y, Chen T, et al. (2016) The effect of AlF_3 modification on the physicochemical and electrochemical properties of Li-rich layered oxide. *Ceram Int* 42: 5397–5402.
55. Jackson DHK (2016) Optimizing AlF_3 atomic layer deposition using trimethylaluminum and TaF_5: Application to high voltage Li-ion battery cathodes. *J Vac Sci Technol A* 34: 031503.
56. Lee HJ, Kim SB, Park YJ (2012) Enhanced electrochemical properties of fluoride-coated $LiCoO_2$ thin films. *Nanoscale Res Lett* 7: 16.
57. Hao S, Wolverton C (2013) Lithium transport in amorphous Al_2O_3 and AlF_3 for discovery of battery coatings. *J Phys Chem C* 117: 8009–8013.
58. Jung SC, Han YK (2013) How do Li atoms pass through the Al_2O_3 coating layer during lithiation in Li-ion batteries? *J Phys Chem Lett* 4: 2681–2685.
59. Xu S, Jacobs RM, Nguyen HM, et al. (2015) Lithium transport through lithium-ion battery cathode coatings. *J Mater Chem A* 3: 17248–17272.
60. Riley LA, Van Atta S, Cavanagh AS, et al. (2011) Electrochemical effects of ALD surface modification on combustion synthesized $LiNi_{1/3}Mn_{1/3}Co_{1/3}O_2$ as a layered-cathode material. *J Power Sources* 196: 3317–3324.
61. Cheng HM, Wang FM, Chu JP, et al. (2012) Enhanced cyclability in lithium ion batteries: resulting from atomic layer deposition of Al_2O_3 or TiO_2 on $LiCoO_2$ electrodes. *J Phys Chem C* 116: 7629–7637.
62. Li X, Liu J, Meng X, et al. (2014) Significant impact on cathode performance of lithium-ion batteries by precisely controlled metal oxide nanocoatings via atomic layer deposition. *J Power Sources* 247: 57–69.
63. Kim JH, Park MH, Song JH, et al. (2012) Effect of aluminum fluoride coating on the electrochemical and thermal properties of $0.5Li_2MnO_3 \cdot 0.5LiNi_{0.5}Co_{0.2}Mn_{0.3}O_2$ composite material. *J Alloy Compd* 517: 20–25.
64. Oi T, Miyauchi K, Uehara K (1982) Electrochromism of $WO_3/LiAlF_4/LiIn$ thin-film overlayers. *J Appl Phys* 53: 1823.
65. Stechert TR, Rushton MJD, Grimes RW, et al. (2012) Predicted structure, thermo-mechanical properties and Li ion transport in $LiAlF_4$ glass. *J Non-Cryst Solids* 358: 1917–1923.
66. Xie J, Sendek AD, Cubuk ED, et al. (2017) Atomic layer deposition of stable $LiAlF_4$ lithium ion conductive interfacial layer for stable cathode cycling. *ACS Nano* 11: 7019–7027.
67. Oi T (1984) Ionic conductivity of LiF thin films containing di- and trivalent metal fluorides. *Mater Res Bull* 19: 451–457.
68. Goodenough JB, Kim Y (2010) Challenges for rechargeable Li batteries. *Chem Mater* 22: 587–603.
69. Goodenough JB, Park KS (2013) The Li-ion rechargeable battery: A perspective. *J Am Chem Soc* 135: 1167–1176.
70. Goodenough JB (2014) Electrochemical energy storage in a sustainable modern society. *Energ Environ Sci* 7: 14–18.
71. Sun YK, Han JM, Myung ST, et al. (2006) Significant improvement of high voltage cycling behavior AlF_3-coated $LiCoO_2$ cathode. *Electrochem Commun* 8: 821–826.

72. Sun YK, Yoon CS, Myung ST, et al. (2009) Role of AlF_3 coating on $LiCoO_2$ particles during cycling to cutoff voltage above 4.5 V. *J Electrochem Soc* 156: A1005–A1010.
73. Aboulaich A, Ouzaoult K, Faqir H, et al. (2016) Improving thermal and electrochemical performances of $LiCoO_2$ cathode at high cut-off charge potentials by MF_3 (M = Ce, Al) coating. *Mater Res Bull* 73: 362–368.
74. Sun YK, Park BC, Yashiro H (2008) Improvement of the electrochemical properties of $Li[Ni_{0.5}Mn_{0.5}]O_2$ by AlF_3 coating. *J Electrochem Soc* 155: A705–A710.
75. Abdel-Ghany A, El-Tawil RS, Hashem AM, et al. (2019) Improved electrochemical performance of $LiNi_{0.5}Mn_{0.5}O_2$ by Li-enrichment and AlF_3 coating. *Materialia* 5: 100207.
76. Woo SU, Yoon CS, Amine K, et al. (2007) Significant improvement of electrochemical performance of AlF_3-coated $Li[Ni_{0.8}Co_{0.1}Mn_{0.1}]O_2$ cathode materials. *J Electrochem Soc* 154: A1005–A1009.
77. Sun YK, Cho SW, Lee SW, et al. (2007) AlF_3-coating to improve high voltage cycling performance of $Li[Ni_{1/3}Co_{1/3}Mn_{1/3}]O_2$ cathode materials for lithium secondary batteries. *J Electrochem Soc* 154: A168–A172.
78. Lee KS, Myung ST, Kim DW, et al. (2011) AlF_3-coated $LiCoO_2$ and $Li[Ni_{1/3}Co_{1/3}Mn_{1/3}]O_2$ blend composite cathode for lithium ion batteries. *J Power Sources* 196: 6974–6977.
79. Park BC, Kim HB, Myung ST, et al. (2008) Improvement of structural and electrochemical properties of AlF_3-coated $Li[Ni_{1/3}Co_{1/3}Mn_{1/3}]O_2$ cathode materials on high voltage region. *J Power Sources* 178: 826–831.
80. Wang HY, Tang AD, Huang KL, et al. (2010) Uniform AlF_3 thin layer to improve rate capability of $LiNi_{1/3}Co_{1/3}$ $Mn_{1/3}O_2$ material for Li-ion batteries. *T Nonferr Metal Soc* 20: 803–808.
81. Shi SJ, Tu JP, Tang YY, et al. (2013) Enhanced electrochemical performance of LiF-modified $LiMn_{1/3}Ni_{1/3}Co_{1/3}O_2$ cathode materials for Li-ion batteries. *J Power Sources* 225: 338–346.
82. Lin H, Yang Y (2009) Structural characterization and electrochemical performance of AlF_3-coated $LiNi_{0.45}Mn_{0.45}Co_{0.10}O_2$ as cathode materials for lithium ion batteries. *Acta Chim Sinica* 67: 104–108.
83. Myung ST, Lee KS, Yoon CS, et al. (2010) Effect of AlF_3 coating on thermal behavior of chemically delithiated $Li_{0.35}[Ni_{1/3}Co_{1/3}Mn_{1/3}]O_2$. *J Phys Chem C* 114: 4710–4718.
84. Song HG, Park YJ (2012) $LiLaPO_4$-coated $Li[Ni_{0.5}Co_{0.2}Mn_{0.3}]O_2$ and AlF_3-coated $Li[Ni_{0.5}Co_{0.2}Mn_{0.3}]O_2$ blend composite for lithium ion batteries. *Mater Res Bull* 47: 2843–2846.
85. Yang K, Fan LZ, Guo J, et al. (2012) Significant improvement of electrochemical properties of AlF_3-coated $LiNi_{0.5}Co_{0.2}Mn_{0.3}O_2$ cathode materials. *Electrochim Acta* 63: 363–368.
86. Amalraj F, Talianker M, Markovsky B, et al. (2013) Studies of Li and Mn-rich $Li_x[MnNiCo]O_2$ electrodes: electrochemical performance, structure, and the effect of the aluminum fluoride coating. *J Electrochem Soc* 160: A2220–A2233.
87. Sun S, Yin Y, Wan N, et al. (2015) AlF_3 surface-coated $Li[Li_{0.2}Ni_{0.17}Co_{0.07}Mn_{0.56}]O_2$ nanoparticles with superior electrochemical performance for lithium-ion batteries. *ChemSusChem* 8: 2544–2550.
88. Xiao QC, Sun KL, Zhang HL, et al. (2014) High performance $Li_{1.2}(Mn_{0.54}Co_{0.13}Ni_{0.13})O_2$ with AlF_3/carbon hybrid shell for lithium ion batteries. *Mater Technol* 29: A70–A76.
89. Deng H, Belharouak I, Yoon CS, et al. (2010) High temperature performance of surface-treated $Li_{1.1}(Ni_{0.15}Co_{0.1}Mn_{0.55})O_{1.95}$ layered oxide. *J Electrochem Soc* 157: A1035–A1039.

90. Zhao T, Chen S, Chen R, et al. (2014) The positive roles of integrated layered-spinel structures combined with nanocoating in low-cost Li-rich cathode $Li[Li_{0.2}Fe_{0.1}Ni_{0.15}Mn_{0.55}]O_2$ for lithium-ion batteries. *ACS Appl Mater Inter* 6: 21711–21720.
91. Li GR, Feng X, Ding Y, et al. (2012) AlF_3-coated $Li(Li_{0.17}Ni_{0.25}Mn_{0.58})O_2$ as cathode material for Li-ion batteries. *Electrochim Acta* 78: 308–315.
92. Ding J, Lu Z, Wu M, et al. (2017) Preparation and performance characterization of AlF_3 as interface stabilizer coated $Li_{1.24}Ni_{0.12}Co_{0.12}Mn_{0.56}O_2$ cathode for lithium-ion batteries. *Appl Surf Sci* 406: 21–29.
93. Rosina KJ, Jiang M, Zeng D, et al. (2012) Structure of aluminum fluoride coated $Li[Li_{1/9}Ni_{1/3}Mn_{5/9}]O_2$ cathodes for secondary lithium-ion batteries. *J Mater Chem* 22: 20602–20610.
94. Wang XY, Ye XH, Zhi XK, et al. (2013) Effects of AlF_3 coating on the electrochemical performance of $Li_{1.2}Mn_{0.52}Ni_{0.2}Co_{0.08}O_2$ cathode materials. *Chinese J Inorg Chem* 29: 774–778.
95. Li Y, Liu KY, Lü MY, et al. (2014) Synthesis, characterization and electrochemical performance of AlF_3-coated $Li_{1.2}(Mn_{0.54}Ni_{0.16}Co_{0.08})O_2$ as cathode for Li-ion battery. *T Nonferr Metal Soc* 24: 3534–3540.
96. Park K, Park JH, Hong SG, et al. (2016) Induced AlF_3 segregation for the generation of reciprocal Al_2O_3 and LiF coating layer on self-generated $LiMn_2O_4$ surface of over-lithiated oxide based Li-ion battery. *Electrochim Acta* 222: 830–837.
97. Zhao S, Sun B, Yan K, et al. (2018) Aegis of lithium-rich cathode materials via heterostructured $LiAlF_4$ coating for high-performance lithium-ion batteries. *ACS Appl Mater Inter* 10: 33260–33268.
98. Chen D, Tu W, Chen M, et al. (2016) Synthesis and performances of Li-rich@AlF_3@graphene as cathode of lithium ion battery. *Electrochim Acta* 193: 45–53.
99. Zhu L, Liu Y, Wu W, et al. (2015) Surface fluorinated $LiNi_{0.8}Co_{0.15}Al_{0.05}O_2$ as a positive electrode material for lithium ion batteries. *J Mater Chem A* 3: 151456–15162.
100. Kim HB, Park BC, Myung ST, et al. (2008) Electrochemical and thermal characterization of AlF_3-coated $Li[Ni_{0.8}Co_{0.15}Al_{0.05}]O_2$ cathode in lithium-ion cells. *J Power Sources* 179: 347–350.
101. Park BC, Kim HB, Bang HJ, et al. (2008) Improvement of electrochemical performance of $Li[Ni_{0.8}Co_{0.15}Al_{0.05}]O_2$ cathode materials by AlF_3 coating at various temperatures. *Ind Eng Chem Res* 47: 3876–3882.
102. Zhang L, Luo F, Wang J, et al. (2014) Surface coating and electrochemical properties of $LiNi_{0.8}Co_{0.15}Al_{0.05}O_2$ cathode in lithium-ion cells. *Adv Mater Res* 1058: 317–320.
103. Lee SH, Yoon CS, Amine K, et al. (2013) Improvement of long-term cycling performance of $Li[Ni_{0.8}Co_{0.15}Al_{0.05}]O_2$ by AlF_3 coating. *J Power Sources* 234: 201–207.
104. Lee DJ, Lee KS, Myung ST, et al. (2011) Improvement of electrochemical properties of $Li_{1.1}Mn_{1.85}Al_{0.05}O_4$ achieved by an AlF_3 coating. *J Power Sources* 196: 1353–1357.
105. Liu H, Tang D (2009) The effect of nanolayer AlF_3 coating on $LiMn_2O_4$ cycle life in high temperature for lithium secondary batteries. *Russ J Electrochem* 45: 762–764.
106. Tron A, Park YD, Mun J (2016) AlF_3-coated $LiMn_2O_4$ as cathode material for aqueous rechargeable lithium battery with improved cycling stability. *J Power Sources* 325: 360–364.
107. Liu Y, Lv J, Fei Y, et al. (2013) Improvement of storage performance of $LiMn_2O_4$/graphite battery with AlF_3-coated $LiMn_2O_4$. *Ionics* 19: 1241–1246.

108. Wang MS, Wang J, Zhang J, et al. (2015) Improving electrochemical performance of spherical $LiMn_2O_4$ cathode materials for lithium ion batteries by Al-F codoping and AlF_3 surface coating. *Ionics* 21: 27–35.
109. Zhu Z, Cai F, Yu J (2016) Improvement of electrochemical performance for AlF_3-coated $Li_{1.3}Mn_{4/6}Ni_{1/6}Co_{1/6}O_{2.40}$ cathode materials for Li-ion batteries. *Ionics* 22: 1353–1359.
110. Wu Q, Yin Y, Sun S, et al. (2015) Novel AlF_3 surface modified spinel $LiMn_{1.5}Ni_{0.5}O_4$ for lithium-ion batteries: performance characterization and mechanism exploration. *Electrochim Acta* 158: 73–80.
111. Li J, Zhang Y, Li J, et al. (2011) AlF_3 coating of $LiNi_{0.5}Mn_{1.5}O_4$ for high-performance Li-ion batteries. *Ionics* 17: 671–675.
112. Ke X, Zhao Z, Liu J, et al. (2016) Spinel oxide cathode material for high power lithium ion batteries for electrical vehicles. *Energy Procedia* 88: 689–692.
113. Ochsner A, Murch GE, Shokuhfar A, et al. (2009) Improvement of the electrochemical properties in nano-sized Al_2O_3 and AlF_3-coated $LiFePO_4$ cathode materials. *Defect Diffusion Forum* 297–301: 906–911.
114. Song GM, Wu Y, Liu G, et al. (2009) Influence of AlF_3 coating on the electrochemical properties of $LiFePO_4$/graphite Li-ion batteries. *J Alloy Compd* 487: 214–217.
115. Tron A, Jo YN, Oh SH, et al. (2017) Surface modification of the $LiFePO_4$ cathode for the aqueous rechargeable lithium ion battery. *ACS Appl Mater Inter* 9: 12391–12399.
116. Wang Y, Qiu J, Yu Z, et al. (2018) AlF_3-modified $LiCoPO_4$ for an advanced cathode towards high energy lithium-ion battery. *Ceram Int* 44: 1312–1320.
117. Ding F, Xu W, Choi D, et al. (2012) Enhanced performance of graphite anode materials by AlF_3 coating for lithium-ion batteries. *J Mater Chem* 22: 12745–12751.
118. Xu W, Chen X, Wang W, et al. (2013) Simply AlF_3-treated $Li_4Ti_5O_{12}$ composite anode materials for stable and ultrahigh power lithium-ion batteries. *J Power Sources* 236: 169–174.
119. Li W, Li X, Chen M, et al. (2014) AlF_3 modification to suppress the gas generation of $Li_4Ti_5O_{12}$ composite anode battery. *Electrochim Acta* 139: 104–110.
120. Liang G, Pillai AS, Peterson VK, et al. (2018) Effect of AlF_3-coated $Li_4Ti_5O_{12}$ on the performance and function of the $LiNi_{0.5}Mn_{1.5}O_4||Li_4Ti_5O_{12}$ full battery—An in operando neutron powder diffraction study. *Front Energy Res* 6: 89.
121. Kim JW, Kim DH, Oh DY, et al. (2015) Surface chemistry of $LiNi_{0.5}Mn_{1.5}O_4$ particles coated by Al_2O_3 using atomic layer deposition for lithium-ion batteries. *J Power Sources* 274: 1254–1262.
122. Han JM, Myung ST, Cho SW, et al. (2006) Significant of AlF_3-coated $LiCoO_2$ cathode in high voltage cycling. *Extended Abstract of the 210th ECS Meeting*, Cancun, Mexico.
123. Makimura Y, Ohzuku T (2003) Lithium insertion material of $LiNi_{1/2}Mn_{1/2}O_2$ for advanced lithium-ion batteries. *J Power Sources* 119–121: 156–160.
124. Lin H, Zheng J, Yang Y (2010) The effects of quenching treatment and AlF_3 coating on $LiNi_{0.5}Mn_{0.5}O_2$ cathode materials for lithium-ion battery. *Mater Chem Phys* 119: 519–523.
125. Amalraj F, Sclar H, Shilina Y, et al. (2018) Horizons for Li-ion batteries relevant to electro-mobility: high-specific-energy cathodes and chemically active separators. *Adv Mater* 30: 1801348.
126. Zhao F, Mu D, Hou X, et al. (2015) Co-effect of AlF_3 and MgF_2 on the electrochemical performance of $LiNi_{0.5}Mn_{0.3}Co_{0.2}O_2$ cathode material under high voltage. *Adv Mater Res* 1088: 327–331.

127. Nayak PK, Erickson EM, Schipper F, et al. (2018) Review on challenges and recent advances in the electrochemical performance of high capacity Li- and Mn-rich cathode materials for Li-ion batteries. *Adv Energy Mater* 8: 1702397.
128. Schipper F, Nayak PK, Erickson EM, et al. (2017) Studies of cathode materials for lithium-ion batteries: recent progress and new challenges. *Inorganics* 5: 32.
129. Li H, Cormier M, Zhang N, et al. (2019) Is cobalt needed in Ni-rich positive electrode materials for lithium ion batteries? *J Electrochem Soc* 166: A429–A439.
130. Park J, Seo JH, Plett G, et al. (1993) Numerical simulation of the effect of the dissolution of $LiMn_2O_4$ particles on Li-ion battery performance. *Electrochem Solid-State Lett* 14: A14–A18.
131. Oh RG, Hong JE, Yang WG, et al. (2015) Effects of Al_2O_3 and AlF_3 coating on the electrochemical performance of $Li_3V_2(PO_4)_3$/C cathode material in lithium ion batteries. *Solid State Ionics* 283: 131–136.
132. Hovington P, Lagacé M, Guerfi A, et al. (2015) New lithium metal polymer solid state battery for an ultrahigh energy: nano C-$LiFePO_4$ versus nano $Li_{1.2}V_3O_8$. *Nano Lett* 15: 2671–2678.
133. Wang H, Yu Y, Jin G, et al. (2013) AlF_3 coated LiV_3O_8 nanosheets with significantly improved cycling stability as cathode material for Li-ion battery. *Solid State Ionics* 236: 37–42.
134. Julien CM, Mauger A (2018) *In situ* Raman analyses of electrode materials for Li-ion batteries. *AIMS Mater Sci* 5: 650–698.
135. Julien CM (2000) 4-volt cathode materials for rechargeable lithium batteries wet-chemistry synthesis, structure and electrochemistry. *Ionics* 6: 30–46.
136. Julien CM, Massot M (2003) Lattice vibrations of materials for lithium rechargeable batteries III. Lithium manganese oxides. *Mat Sci Eng B-Adv* 100: 69–78.
137. Gross U, Rüdiger S, Kemnitz E, et al. (2007) Vibrational analysis study of aluminum trifluoride phases. *J Phys Chem A* 111: 5813–5819.
138. Boulard B, Jacoboni C, Rousseau M (1989) Raman spectroscopy vibrational analysis of octahedrally coordinated fluorides: Application to transition metal fluoride glasses. *J Solid State Chem* 80: 17–31.
139. Makarowicz A, Bailey CL, Weiher N, et al. (2009) Electronic structure of Lewis acid sites on high surface area aluminium fluorides: a combined XPS and ab initio investigation. *Phys Chem Chem Phys* 11: 5664–5673.
140. Tatara R, Karayaylali P, Yu Y, et al. (2019) The effect of electrode-electrolyte interface on the electrochemical impedance spectra for positive electrode in Li-ion battery. *J Electrochem Soc* 166: A5090–A5098.
141. Kendig M, Scully J (1990) Basic aspects of electrochemical impedance application for the life prediction of organic coatings on metals. *Corrosion* 46: 22–29.
142. Fletcher S (1994) Tables of degenerate electrical networks for use in the equivalent-circuit analysis of electrochemical systems. *J Electrochem Soc* 141: 1823–1826.
143. Zheng JM, Zhang ZR, Wu XB, et al. (2008) The effects of AlF_3 coating on the performance of $Li[Li_{0.2}Mn_{0.54}Ni_{0.13}Co_{0.13}]O_2$ positive electrode material for lithium-ion battery. *J Electrochem Soc* 155: A775–A782.
144. Li D, Sasaki Y, Kobayakawa K, et al. (2006) Preparation and electrochemical characteristics of $LiNi_{1/3}Mn_{1/3}Co_{1/3}O_2$ coated with metal oxides coating. *J Power Sources* 160: 1342–1348.
145. Kang SH, Amine K (2007) Layered cathode materials for lithium ion rechargeable batteries. US Patent 7,205,072B2.

146. Gallagher KG, Nelson PA, Dees DW (2011) Simplified calculation of the area specific impedance for battery design. *J Power Sources* 196: 2289–2297.
147. Belharouak I, Sun YK, Liu J, et al. (2003) $Li(Ni_{1/3}Co_{1/3}Mn_{1/3})O_2$ as a suitable cathode for high power applications. *J Power Sources* 123: 247–252.
148. Son JT (2008) Improvement of electrochemical properties of surface modified $Li_{1.05}Ni_{0.35}Co_{0.25}Mn_{0.4}O_2$ cathode material for lithium secondary battery. *B Korean Chem Soc* 29: 1695–1698.
149. Klett M, Gilbert JA, Pupek KZ, et al. (2017) Layered oxide, graphite and silicon-graphite electrodes for lithium-ion cells: Effect of electrolyte composition and cycling windows. *J Electrochem Soc* 164: A6095–A6102.
150. Shim J, Striebel KA (2003) Characterization of high-power lithium-ion cells during constant current cycling: Part I. Cycle performance and electrochemical diagnostics. *J Power Sources* 122: 188–194.
151. Nakura K, Ariyoshi K, Ogaki F, et al. (2014) Characterization of lithium insertion electrodes: a method to measure area-specific impedance of single electrode. *J Electrochem Soc* 161: A841–A846.
152. Mauger A, Julien CM (2017) Critical review on lithium-ion batteries: are they safe? Sustainable? *Ionics* 23: 1933–1947.
153. Wang MS, Wang J, Zhang J, et al. (2015) Improving electrochemical performance of spherical $LiMn_2O_4$ cathode materials for lithium ion batteries by Al-F codoping and AlF_3 surface coating. *Ionics* 21: 27–35.
154. Tron A, Kang H, Kim J, et al. (2018) Electrochemical performance of AlF_3-coated LiV_3O_8 for aqueous rechargeable lithium-ion batteries. *J Electrochem Sci Te* 9: 60–68.

AIMS Press